Deep Tissue Optical and Optoacoustic Molecular Imaging Technologies for Small Animal Research and Drug Discovery

Daniel Razansky[1,*], Nikos Deliolanis[1], Claudio Vinegoni[2] and Vasilis Ntziachristos[1]

[1]*Institute for Biological and Medical Imaging (IBMI), Technical University of Munich and Helmholtz Center Munich, Ingoldstädter Landstraße 1, 85764 Neuherberg, Germany;* [2]*Center for Systems Biology, Massachusetts General Hospital, Harvard Medical School, 185 Cambridge Street, Boston, MA 02114, USA*

Abstract: For centuries, biological discoveries were based on optical imaging, in particular microscopy but also several chromophoric assays and photographic approaches. With the recent emergence of methods appropriate for bio-marker *in vivo* staining, such as bioluminescence, fluorescent molecular probes and proteins, as well as nanoparticle-based targeted agents, significant attention has been shifted toward *in vivo* interrogations of different dynamic biological processes at the molecular level. This progress has been largely supported by the development of advanced tomographic imaging technologies suitable for obtaining volumetric visualization of bio-marker distributions in small animals at a whole-body or whole-organ scale, an imaging frontier that is not accessible by the existing tissue-sectioning microscopic techniques due to intensive light scattering beyond the depth of a few hundred microns. Major examples of such recently developed optical imaging modalities are reviewed here, including bioluminescence tomography (BLT), fluorescence molecular tomography (FMT), and optical projection tomography (OPT). The pharmaceutical imaging community has quickly appropriated itself of these novel forms of optical imaging, since they come with very compelling advantages, such as quantitative three-dimensional capabilities, direct correlation to the biological cultures, easiness and cost-effectiveness of use, and the use of safe non-ionizing radiation. Some multi-modality approaches, combining light with other imaging modalities such as X-Ray CT or MRI, giving the ability to acquire both an optical contrast reconstruction along with a hi-fidelity anatomical images, are also reviewed. A separate section is devoted to the hybrid imaging techniques based on the optoacoustic phenomenon, such as multispectral optoacoustic tomography (MSOT), which are poised to leverage the traditional contrast and specificity advantages of optical spectrum by delivering an ever powerful set of capabilities, including real-time operation and high spatial resolution, not affected by the scattering nature of biological tissues.

Keywords: Optical molecular imaging, drug discovery, optoacoustic tomography, small animals, contrast agents, *in-vivo* imaging.

1. INTRODUCTION

Optical imaging is a key tool for the understanding of gene function, the study of pharmacokinetics and to follow drug delivery and barrier penetration. In the modern drug development arena, with more than 10 years and almost US$1 billion currently spent on average for bringing a single new drug to a safe and approved human use[1], imaging capabilities become increasingly essential for early selection of promising new drug candidates and for accelerating the overall drug discovery and development processes, thus also saving significant costs. Unfortunately, for all cases where it is necessary to follow the dynamics and coordination in whole living organisms, traditional optical imaging techniques are not adequate. Optical microscopy in particular has been an essential tool for biomedical research but, when dealing at the organ or whole organism level, it has focused mostly on the study of dead specimen, i.e. through histology or immunohistochemistry. With time, a stronger need to study evolution, function and disease in unperturbed environment led to the development of all current *in vivo* optical imaging modalities.

*Address correspondence to this author at the Institute for Biological and Medical Imaging (IBMI), Technische Universität München and Helmholtz Zentrum München, Ingolstädter Landstraβe 1, 85764 Neuherberg, Germany; Tel: +49-89-3187-1587, Fax: +49-89-3187-3063; E-mail: dr@tum.de

Early optical imaging systems, which attempted deep-tissue imaging, were confronted with the intrinsic limitations associated with single-projection acquisition, such as non-quantitative ability and low resolution, especially when aiming at attaining non-superficial optical contrast. An important physical difference that exist between obtaining microscopic images of a few cell monolayers or thin histological slices and imaging instead whole tissue or organs in small animals or humans is scattering: thick tissues diffuse light and significantly reduce the resolution and the overall image fidelity. When light encounters thick tissues, photons interact with cellular interfaces and organelles leading to multiple changes in direction (scattering events) within the specimen under investigation [2]. The detected light therefore loses information on its origin and propagation path, blurring the images and destroying spatial resolution. Even state of the art multiphoton microscopy [3] is usually limited to superficial imaging up to a depth of 0.5-1 mm in most living tissues. Some recent techniques, such as optical projection tomography, selective-plane illumination microscopy or ultramicroscopy can image entire embryos or intact organs however they require naturally transparent specimen [4] or special chemical treatment to clear them from scattering [5], which is only suitable for post-mortem imaging.

Macroscopic optical imaging has recently evolved as an alternative for visualizing large diffuse specimen. It uses

1389-2010/12 $58.00+.00

fully diffusive photons, typically from objects that are larger than 1 cm. In its advanced form, techniques like Fluorescence Molecular Tomography (FMT) illuminate the sample under investigation at multiple projections and utilize mathematical models of photon propagation in tissues to reconstruct the underlying imaging contrast6. In contrast to microscopic three-dimensional "tissue-sectioning" imaging, *tomography* and *reconstruction* here implies the formulation of a mathematical inverse problem, whose algebraic solution yields the reconstructed images, in analogy to methods used in X-ray CT, Single Tomography (PET). Several different implementations, developed over the past years, have been successfully used to three-dimensionally image bio-distribution of fluorochromes in whole small animals, molecular pathways of cancer and cardiovascular disease, and to offer quantitative imaging. However the price to pay when applying a light diffusion model is poor spatial resolution, which is always exchanged for penetration. Therefore, as the size of the imaged object grows, imaging resolution quickly deteriorates [7]. It is indeed possible to perform optical tomography, such as FMT, through entire mice with high sensitivity, but low resolution ability of about 1mm or worse [8].

In response, optical imaging experienced a slow and bumpy propagation into the biological practice over the last two decades. Recent developments however put forth technologies that not only rise above the issues of the past but come with features that challenge even well established imaging modalities typically considered in the pharmaceutical discovery. In particular, multi-modality images approaches combining optical tomographic systems with high resolution modalities such as X-Ray CT or MRI give the ability to acquire both highly specific molecular information and a hi-fidelity anatomical image that can be co-registered [6,9-18]. The anatomical information can be used in making assumptions on the relationship between tissue structures and optical properties and also on the precise spatial distribution of fluorescent probes. Another emerging modality is multi-spectral opto-acoustic tomography (MSOT) [19-21], a new technique that possesses highly diverse abilities to detect optical reporter molecules and tissue biomarkers at high resolution, not affected by photon scattering. With versatility and sensitivity common to nuclear imaging, imaging speed that can only be found in ultrasound as well as good anatomical contrast and spatial resolution typical to X-ray CT and magnetic resonance imaging, MSOT is ideally suited for imaging of cellular and sub-cellular activity at the whole body level.

2. EX VIVO WHOLE BODY/ORGAN METHODS AND IMAGING IN LOW DIFFUSION REGIME

As previously mentioned, diffusive properties of biological tissues impose limitations on resolution and penetration depth that are currently achievable by optical tomography techniques. When aiming at *in-vivo* studies, this drawback can be tolerated in view of the possibility to obtain valuable information during longitudinal studies. But for all those cases where high resolution is needed, other approaches involving *ex-vivo* studies could become a valuable alternative.

2.1. Volumetric Visualization of Cryo-Sliced Tissues

In many cases, confirmation of *in-vivo* findings and overall the study of fluorochrome bio-distribution in different organs is based on *ex-vivo* fluorescence imaging of excised organs, typically placed under a fluorescence camera [22]. This approach comes with several limitations, most notably the absence of truly volumetric data throughout the organs imaged, the loss of accurate information as to the organs surrounding tissues and as a result also the possible omission of unknown areas of fluorochrome accumulation. A particular limitation is the inability of fluorescence planar imaging to image below the surface, therefore *ex-vivo* imaging of excised organs only reflects the fluorochrome bio-distribution at the surface of the organ imaged. As a result, little is known as to the exact whole body bio-distribution of many fluorescently labeled agents used for exploratory or therapeutic purposes.

For this reason, cryo-slicing imaging systems have been developed to study and validate the bio-distribution of fluorescent probes for *in-vivo* small animal imaging. Most such systems are based on a conventional cryoslicer unit retrofitted with fluorescence camera while multiple adjacent slices, previously obtained by cryo-sectioning, are combined together via image processing to obtain volumetric information [23-25]. Most recently developed systems use fully automated sectioning with multiple-wavelength capturing camera and can quickly resolve multiple fluorochromes in the same measurement for comparative studies [26]. By using this type of spectral differentiation one becomes capable of identifying not only the particulars of bio-distribution but also the relative accumulation of a targeted agent or several agents simultaneously. In parallel, the auto-fluorescence present in mouse tissues is also investigated and plotted in direct relation to the signals obtained from the probes for comparison reasons. Finally, Monte Carlo methods for light attenuation correction could be further used to improve the image quality for out-of-focus fluorochrome locations.

2.2. Optical Projection Tomography

While the cryo-slicing methodology provides exquisite resolution in combination with the ability to obtain both fluorescence and staining information, it usually induces severe structural artifacts due to the freezing and cutting procedures. An alternative technique capable of providing similar resolutions without requiring any physical sectioning is optical projection tomography (OPT) [5,27,28], a three-dimensional imaging technique that is particularly well suited for developmental biology and gene expression studies. OPT is the optical equivalent of X-ray computed tomography and it works under the approximation of negligible light scattering. For biological samples this condition is achieved via chemical treatment that consists of replacing the cellular fluids with a solution index matching the cell membranes, which also removes de facto most of tissue scattering contributions. During this procedure, the samples are first dehydrated and then placed for several hours in a clearing solution where they become optically transparent. Once cleared, fluorescent and/or absorption images are acquired in transillumination mode over 360 degrees by rotating the sample along its vertical axis. A high telecentric lens com-

bined with a diaphragm with variable aperture collects photons with a travel path parallel to its optical axis. This condition ensures that algorithms commonly used for X-CT such as Radon backprojection can be successfully implemented in order to obtain absorption maps. Schematic representation of the OPT tomographic principle is presented in Fig. (**1**) along with the other optical and optoacoustic imaging methods discussed in this paper.

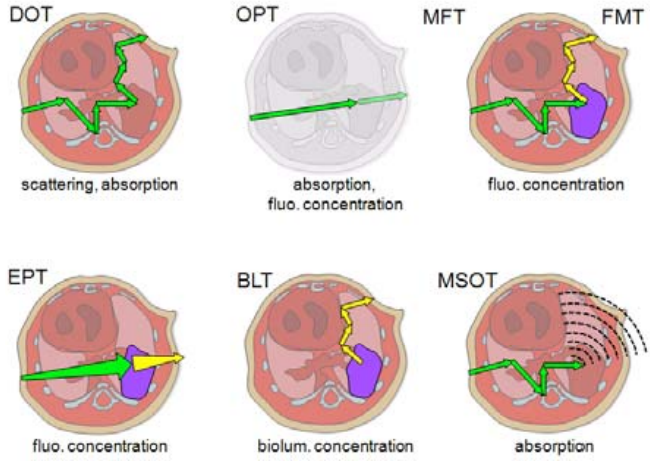

Fig. (1). Schematic representation of the main optical and optoacoustic tomographic methods used for deep tissue imaging.

OPT has been proven ideal for describing and rendering antibody-stained tissue in embryionic organs Fig. (**2**). In addition to small animal embryo imaging, OPT has been also demonstrated for whole organ imaging, such as heart and lung. Of particular interest is the possibility to obtain high resolution tomographic information relative to the distribution of several smart activatable fluorescent optical agents capable of providing molecular information. This option is very attractive in a way that allows complementing, at a different resolution scale, information previously collected with *in vivo* imaging techniques such as FMT or MSOT.

Yet, most organs present a varying spatially dependent level of absorption, making incorrect the use of the Radon algorithm for backprojecting the fluorescence images. A normalized Born ratio for fluorescence OPT based on a transillumination approach has been recently proposed [29], demonstrating performance improvements over conventional fluorescence OPT for both phantoms and whole hearts of mice. Transillumination in both fluorescence and absorption mode are collected over 360 degrees and the normalized Born intensity U_B, defined as the ratio of fluorescence over the corresponding excitation measurements, is introduced. Once the correct Green's functions for both the excitation and emission photons are defined, the tomographic set of Born normalized measurements can be then expressed as $U_B = WA$, where W and A represent the forward model matrix and volumetric distribution of the fluorophores. The latter can subsequently be extracted by applying the Radon backprojection to the set of measurements U_B. Distribution of Prosense-680, an activatable fluorescence sensor that reports on cathepsin activity in the healing myocardium, has been obtained for a whole heart that had previously sustained a controlled infarct Fig. (**3**). Due to the high absorption values present in the heart, a born normalized approach is necessary to obtain the correct fluorophore distribution maps. In addition to cathepsin activity, OPT has been demonstrated for

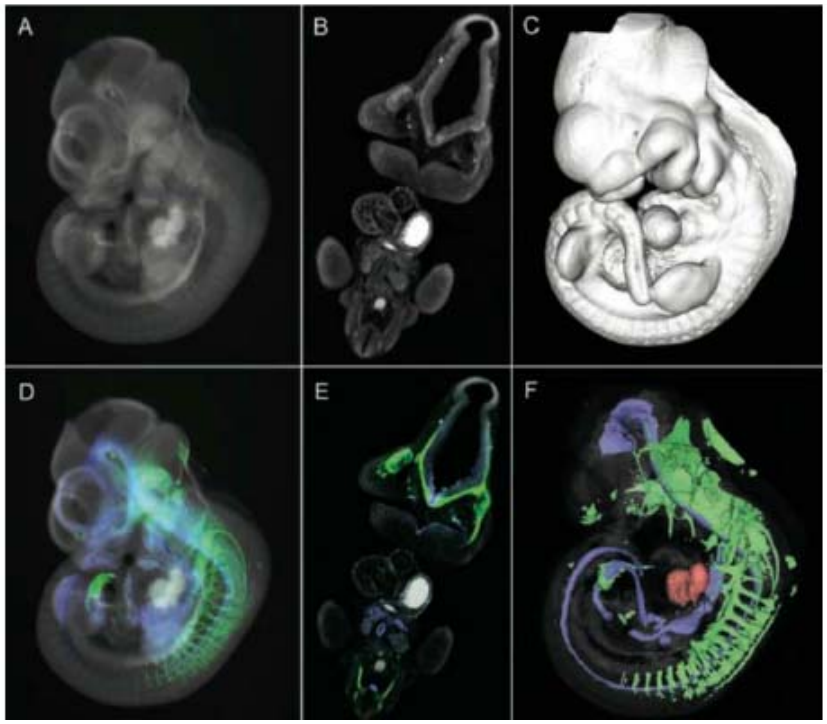

Fig. (2). Fluorescence OPT signal of an E10.5 mouse embryio stained with HNF3B antibodies. (**A**) Autofluorescence projection; (**B**) Axial section of autofluorescent signal; (**C**) 3D rendering of an iso-surface; (**D** to **F**) Equivalent views as in A,B, and C with overlaid fluorescence signal of the double-antibody staining. Reprinted with permission from Ref [5]. ©2010 American Association for the Advancement of Science.

detecting enzyme activity mediated by eosinophils in mice with inflamed lungs [30], a model extremely valuable to study allergen exposure Fig. (**4**). In this model a NIR metalloproteinase (MMP)-targeted sensor has been used to monitor the eosinophyl-mediated inflammation.

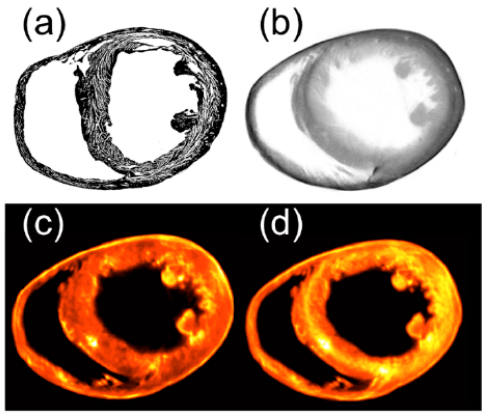

Fig. (3). Reconstructions of a mouse heart that had previously sustained a controlled infarct. (**a**) Histology, (**b**) absorption reconstruction, (**c**) plain fluorescence reconstruction, and (**d**) normalized Born fluorescence reconstruction of the Prosense-680 probe signal. Reprinted with permission from Ref [29]. ©2009 Optical Society of America.

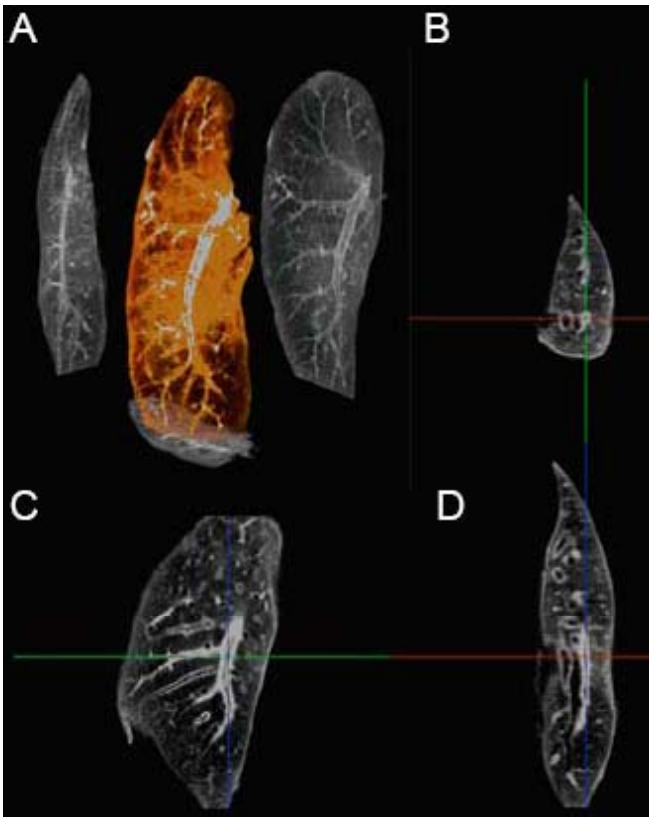

Fig. (4). Lung fluorescence distribution reconstructions of an OVA-challenged mouse injected with MMPsense 680. (**a**) Three-dimensional lung reconstruction; (**b**)–(**d**) coronal, axial, and saggital sections. Reprinted with permission from Ref [30]. ©2010 Optical Society of America.

The capability to obtain molecularly sensitive imaging contrast in OPT by means of targeted and activatable imaging reporter agents provides therefore a great tool for investigating the molecular signatures of pathophysiological processes and to study different inflammatory responses as a function of drug dosage. Despite these significant improvements, until recently high throughput imaging remained restricted, with major limiting factor being the time necessary for obtaining three-dimensional tomographic reconstructions. A possible solution to this bottleneck became available with the introduction of parallel processing Radon-backprojection platform, implementing graphic processing unit (GPU) [31], which has been proven to provide a 300 fold performance enhancement in comparison to the CPU workstation implementations. This new technology now offers the ability to obtain on-the-fly reconstructions and thus enables high-throughput capability Fig. (**5**).

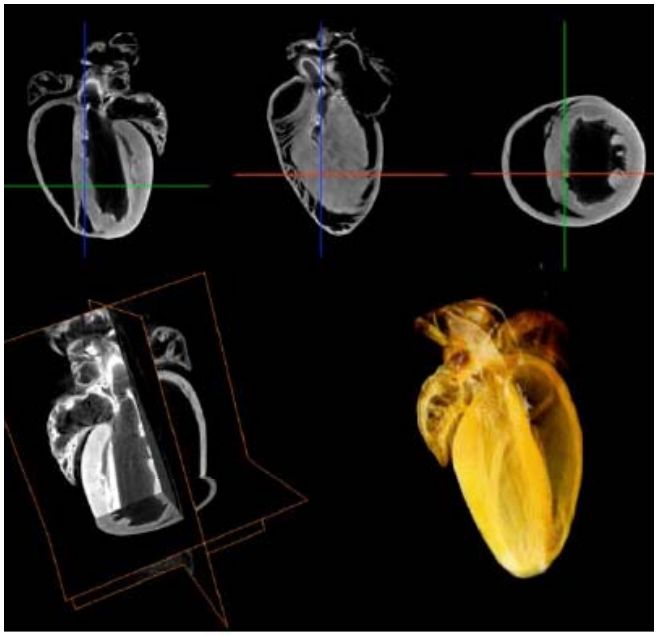

Fig. (5). Heart tomographic reconstructions by absorption OPT obtained using GPU. The reconstructions are made using 360 projections and are obtained in 65 seconds with read and write on-disk operation. Selected sections of the reconstructed images at three different planes are presented too. The size of each projection corresponds to 1024x1024 pixels. Reprinted with permission from Ref[31]. ©2009 Optical Society of America.

2.3. Light Sheet Microscopy

A different method of optical tomography, the selective plane illumination microscopy (SPIM), which is also applicable for three-dimensional visualization of large specimen, was recently suggested [4]. Several analogous implementations have been also later demonstrated under the name of ultramicroscopy [32]. The general principle is based on an optical equivalent of tissue sectioning and utilizes sample illumination with a sheet of light obtained by way of a cylindrical lens. Images are then acquired in both fluorescence or absorption modes, ortogonally to the plane of illumination, by using an imaging lens or an objective coupled to a CCD.

The illuminating plane is then scanned vertically by way of a motorized tranlation stage or with a set of galvanometers and the entire sample is concomitantly imaged providing tomographic reconstructions. Depending on the size of the sample ,objectives with low or high magnification can be used and different ranges of resolution can be easily achieved. While the lateral resolution is ultimately related to the magnification and the numerical aperture of the objective used, the axial resolution is given by the thickness of the illuminating plane. The major advantage of the technique with respect to other scanning microscopic techniques and OPT resides in its intrinsic ability to acquire single axial planes from large volumes (several mm and beyond) at once without scanning any imaging beam. This implies faster (real-time) acquisition times and less photobleaching, making SPIM particularly suited for following fast biological events at single micron resolution in large specimen. It has been proven efficient for imaging of small insects (Drosophila) or transparent animals (Mekada fish), as shown in Fig. (**6**) A-C. In general, since SPIM is also based on light detection, scattering will still affect its resolution making it not particularly indicated for imaging of non-transparent organisms. A chemical clearing procedure, such as the one exploited for OPT, is therefore required in order to image through the entire sample while maitaning a micron level resolution and several applications for brain or whole mouse embryo imaging Fig. (**6 D-G**) have been recently proven [32].

2.4. Mesoscopic Fluorescence Tomography

When *in vivo* imaging is of interest, e.g. in longitudinal molecular imaging or studies aiming at tracking morphogenesis of a living organism, the tissue, naturally, cannot be sliced nor cleared from scattering. Furthermore, as the size of the imaged area/object grows, the approaches, based on hardware rejection of highly scattering photons, become less efficient since they are mainly suited for operation at depths that are less than one transport mean free path-length MFP (i.e. the distance a photon travels before losing memory of its origin), which translates to biological samples with dimensions of the order of about 0.5 – 1 mm. On the other hand, other macroscopic optical imaging modalities such as Fluorescence Molecular Tomography, which will be discussed in the following chapter, can only effectively be applied in fully-diffusive regime, i.e. to samples much larger then a transport mean free path (5-10 mm).

A new recently introduced imaging technique, Mesoscopic Fluorescence Tomography [7], aims at filling this imaging gap particularly for fluorescence tomographic longitudinal studies of relatively small organisms and tissues, such as developing insects, small animal extremities and embryos, thus, allows to follow dynamic molecular and functional phenomena over time on the same living organism. For instance some developing insects, such as Drosophila melanogaster, have extremely low costs in maintenance while both presenting small size, high fertility rate, and fast development. D. melanogaster has been therefore become particularly attractive as an animal model for pharmacokinetics studies in order to validate high-throughput screening of several compounds creating a need for new optical imaging modalities capable of providing whole body imaging.

The experimental setup of Mesoscopic Fluorescence Tomography has many similarities to other optical tomographic techniques. Light from a CW laser is beam expanded and then collimated to fill the back aperture of a low numerical aperture objective before illuminating the sample under investigation. The sample is then rotated along its vertical axis

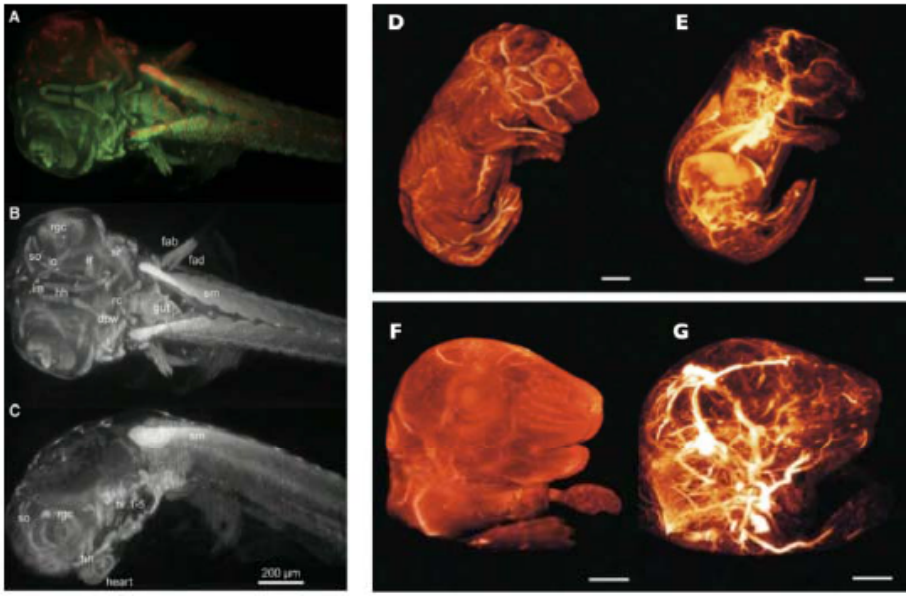

Fig. (6). *In vivo* high resolution image of a Mekada embryio (1549 x 850 x 888 microns) obtained with SPIM. (**A**) Overlay and fusion of different stacks obtained separately. Maximum single projections are shown instead in (**B**) and (**C**) for dorsal-ventral and lateral views. The obtained high resolution allows to clearly distinguish different tissues such as retinal ganglian cells (rgc), fin adductor (fad), transverse ventrals (tv), etc. SPIM reconstructions of a clear whole embryio (ex vivo) is presented in D-G. (**D**) Surface rendering of the embryio and (**E**) the corresponding vascular system. (**F**) Surface rendering of the mouse embyrio's head with (**G**) the corresponding vasculature. Reprinted with permission from Ref [4] ©2004 American Association for the Advancement of Science (AAAS) and Ref [32] ©2007 Macmillan Publishers Ltd.

and multiple images are collected in transillumination mode using an imaging system coupled to a CCD camera. Different filters can be selected and both absorption and/or fluorescence signals can be collected. The internal fluorescence distribution can be obtained in a similar fashion as for FMT, by selecting an appropriate model that describes the photon propagation within the specific sample. Once solved the forward problem, it can be inverted by using the algebraic reconstruction technique and tomographic reconstructions can be obtained.

The Fermi simplification to the Fokker-Planck solution of photon transport theory has been proven to be appropriate in order to model the photon propagation within organisms with sizes equal to approximately 1 MFP such as D. melanogaster [7]. The feasibility of this approach has been successfully proven and tomographic reconstructions of GFP-salivary glands in a Drosophila's pupa have been obtained Fig. (**7a**). Moreover the possibility to obtain time-lapse studies over several hours has been demonstrated providing a valuable and unique tool for longitudinal *in vivo* studies. Fig. (**7b**) shows axial reconstructions of GFP-expressing wing imaginal discs in D. melanogaster pupae during the first 7 hours of pupariation while providing the corresponding matching histology, validating the use of this novel technique for dynamic *in vivo* studies.

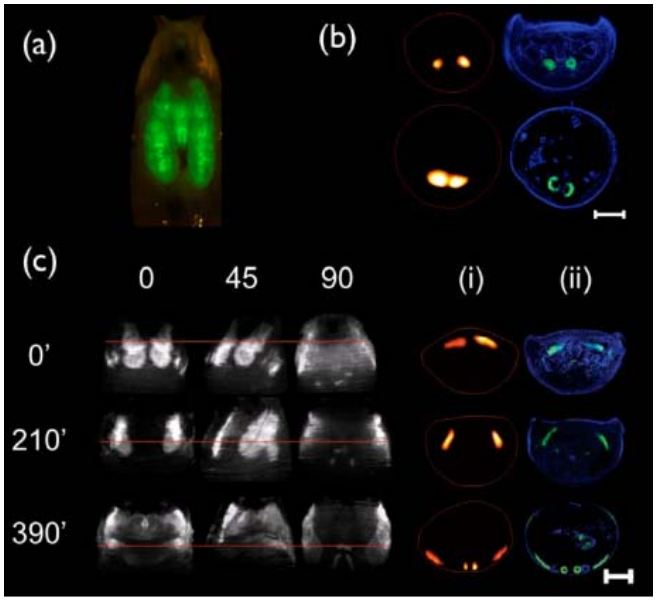

Fig. (7). *In vivo* Mesoscopic Fluorescence Tomographical imaging in Drosophila melanogaster. (**a**) Fluorescence image of GFP-expressing salivary glands overlayed on a pupal case. (**b**) Axial reconstructions of the salivary glands by MFT of a Drosophila melanogaster pupa at two different heights with the corresponding histology. (**c**) Longitudinal study of morphogenetic development of GFP-expressing wing imaginal discs. Fluorescence transillumination projections at three different angles with the corresponding reconstructions and histological sections are presented. Reprinted with permission from Ref [7]. ©2008 Macmillan Publishers Ltd.

Mesoscopic Fluorescence Tomography provides therefore a means for bridging the currently existing *in-vivo* optical imaging gap between microscopy and macroscopy, thus introducing a new way to generate "*in vivo*" three-dimensional fluorescence distributions within optically diffusive non-transparent specimens with sizes up to several millimeters.

3. MOLECULAR IMAGING THROUGH DIFFUSE LIVING TISSUES

3.1. Planar Imaging

In contrast to microscopic-resolution methods and mesoscopy, macroscopic imaging operates at larger scales and the imaged tissues range from the opaque organ and system level to whole body imaging in small animals. In the simplest form it uses macro/photographic lenses and cameras that directly image tissues, with the lateral field of view extending up to 10 cm, while the collected photons can emanate from a depth of several centimeters, depending on the tissue absorption. In general, the macroscopic diffuse imaging methods utilize photons that have been scattered multiple times and, as a result, imaging resolution in deep tissues is compromised. Macroscopic diffuse imaging can be generally classified into simple planar imaging techniques, where resolution is highly compromised with depth, and quantitative tomographic methods, where light propagation is modeled and used to predict light source distribution.

Planar imaging is technologically and methodologically a simple technique, in which the photon field emerging from the object is recorded using a high sensitivity photographic system (typically CCD camera with a lens and appropriate filters). In fluorescence imaging, the emitted photon field is acquired with the use of bandpass filters to isolate the emission wavelength and reject the excitation. There are two major imaging configurations, epillumination and transillumination, where the light is incident on tissue from the same or the opposite side to the camera, respectively. Fluorescence reflectance imaging has an advantage when the fluorescence source is close to the surface, such as subcutaneous tumors [33,34]. However, the performance of reflectance imaging quickly deteriorates with imaging depth, because deep seated fluorescence is highly attenuated compared to superficial unspecific signals due for instance to autofluorescence. On the other hand, fluorescence transillumination performs better when imaging in deep tissue due to the more balanced attenuation of deep and superficial images. Significant improvement in the image quality in transillumination imaging is achieved when dividing (normalizing) the fluorescence images with the corresponding ones acquired at the emission wavelength [35,36]. This normalization compensates for the point-to-point variation in the illumination, as well as for the spatially varying tissue absorption. Finally, the experimental setup for planar bioluminescence imaging is simpler than fluorescence, since no illumination is required. However, planar bioluminescence imaging can give only qualitative results, similarly to unnormalized fluorescence imaging.

3.2. Tomographic Optical Diffusion Imaging

In order to address the quantification and penetration limitations of planar imaging, optical tomography combines multiple illumination-detection points and theoretical models of photon propagation to provide the volume distribution of the unknown quantity. Similar to planar imaging, there are

three major variations of optical tomography that operate in fully diffusive regime: Diffuse Optical Tomography (DOT), where the light is scattered and detected at the boundary of tissue to reconstruct the optical properties of the tissue Fig. (**1a**); Fluorescence Molecular Tomography (FMT), in which the distribution of the fluorochrome is reconstructed Fig. (**1b**); Bioluminescence Tomography (BLT) where the luciferase distribution is reconstructed Fig. (**1c**). The resolution achieved in tissue imaging with optical tomographic methods depends primarily on the imaging depth and can range from sub-millimeter for structures located up to 3 mm up to a centimeter for large structures, such as the human breast.

Optical tomography is in general a demanding modeling and computational problem that it is also ill-posed due to the strong light diffusion [37]. This means that the solutions (the spatial distributions of the unknown quantity) may not be unique, that they are sensitive to noise, and can only be reached after regularization. Photon propagation is theoretically modeled utilizing an approximate solution to the radiation transport equation [38]. A common simplification however is to utilize the diffusion approximation which models photon propagation as a diffusion process. There are two steps in optical tomography problems. First, is the set-up of the "forward problem" of photon propagation in tissue, i.e. the calculation of what would be the light intensity detected at the surface of the tissue as a function of the parameters involved in photon propagation (tissue optical properties, fluorescence and luciferace concentration, for DOT, FMT and BLT, respectively). The forward problem is calculated for a set of different initial conditions, for example, light source positions. Subsequently, for obtaining the actual reconstruction, the inverse problem can be solved by an optimization that typically strives to minimize some similarity criterion between the actual data and the forward solution results.

There are various geometrical and methodological implementations of optical tomographic systems. With respect to light modulation, these are classified as a) continuous wave (CW) systems, where the beam intensity is not modulated (BLT can only be considered as CW, since bioluminescence emission is continuous), b) as time domain (TD) systems, where illumination comprises short pulses (typically <10 ps) and detection is based on time-gated imaging, which is able to record the intensity of light as a function of time, and c) frequency domain (FD) systems, where the light intensity is modulated, typically in the 100-1000 MHz range, while the recorded signal is demodulated to resolve amplitude and phase retardation of the signal. Although TD and FD techniques are more complicated both in hardware and data processing, they are capable of resolving the spatially dependent characteristics of photon propagation. TD and FD techniques are reciprocal transformations of the same principle, the main advantage of the FD over TD, is the high rejection ratio of the non-modulated noise components like ambient light and potentially the improved signal to noise ratio of operation.

With respect to imaging geometry, in first tomographic systems the light was delivered and detected with optical fibers that were placed either in direct contact with tissue, or on the walls of imaging chambers filled with optical matching fluids [39-42]. However, over past years, non-contact optical tomographic approaches have prevailed since they have simplified the experimental procedures and increased the size and quality of the collected data [43,44]. Instead of fibers, the imaged tissue stands in free space and its surface is scanned with laser beams and imaged directly using cameras.

In Diffuse Optical Tomography the unknown parameters that are reconstructed are the 3D distributions of the scattering (μ_s') and absorption (μ_a) coefficients of the tissue. The different optical properties in a specimen are associated with different tissue types (such as, muscle, bone, fat), or with particular physiological and disease states, for example tumor, edema, moles etc. CW DOT is a highly ill-posed problem that cannot differentiate scattering from absorption; but TD and FD DOT as well as multispectral imaging can produce datasets that contain information that can help disentangle absorption with scattering. Indeed, multispectral DOT is capable of functional imaging of the oxygen saturation in tissue since the absorption spectra of oxygenated and dis-oxygenated hemoglobin are different [45,46]. Diffuse optical tomography has been used in various *in vivo* applications, such as brain functional studies, stroke monitoring, joint imaging, breast cancer imaging [47-49]. Approaches that improve image reconstruction consider the use of a-priori information, as derived from another high-resolution modality [9] or using multispectral information to improve the ill-posed nature of the inverse problem [45]. However, as DOT is not intended for highly specific imaging of molecular bio-markers, here we have only briefly mentioned its main characteristics and applications.

3.3. Fluorescence Molecular Tomography

As opposed to DOT, forward problems utilized in fluorescence tomography typically need to solve two separate problems that describe the propagation of the excitation and the emitted photons, where the solution of the excitation is used in the emission problem. The solution of the two problems provide the optical properties of tissue and the fluorescence bio-distribution, directly related to the molecular contrast [50-52]. A simple but efficient approach that has simplified the fluorescence tomography problem is the normalized Born approximation [53], which is similar to the normalization of planar fluorescence images with the excitation image that was described before. The main advantages are that the normalization corrects for the spatially dependent gain factors between different sources and detectors, and that it significantly reduces the sensitivity to the background optical heterogeneity, thus offering a method appropriate for *in-vivo* imaging. After normalization the influence of the spatial variation of the unknown optical properties is practically canceled and the algebraic equation that describes the forward model is:

$$U_{\text{nBorn}} = W \cdot C_{\text{fl}}, \tag{1}$$

where U_{nBorn} is a matrix of the normalized measurements, C_{fl} is the unknown fluorescence distribution, and W is a matrix that models the weight (probability) that the fluorescence emitted from a point m is detected at a point d when

illuminated from a point light source on the surface of the imaged object at *s*

$$W = \frac{U_{s\to m} U_{m\to d}}{U_{s\to d}}, \quad (2)$$

where $U_{s\to m}$, $U_{m\to d}$, and $U_{s\to d}$ are the photon intensities from source to the reconstructed mesh, mesh to detector, and source to detector, respectively.

Over the past years, the free-space 360-degree FMT has proven to be highly suitable for *in-vivo* imaging of small animals to study models of disease like cancer, neurological, cardiovascular, inflammation, metabolism etc. *In-vivo* imaging of a mouse model of lung cancer with CW-FMT is shown in Fig. (**8**). The mouse shown was implanted with 1x10 [6] Lewis Lung Carcinoma (LLC) cells administered intercostally into the right lung parenchyma [54]. Twelve days after implantation the mouse received 2 nmol of angiogenesis sensitive fluorescent probe (Angioscence750, Visen Medical) via the tail vein and was imaged 36 hours later. During the experiment the mouse was anesthetized with ketamine and xylazine. The images demonstrate protease imaging in 360-degree free-space FMT mode and co-registered X-ray CT images acquired prior to FMT imaging showing virtually identical mouse placement. The FMT images highlight areas of increased fluorescence concentration congruent with the location of tumor seen on the X-ray CT images. Similar method was applied for visualization of myocardial macrophage infiltration *in vivo* [55]. In this study, the reconstructed coronal slices from the 3-dimensional FMT data set have been superimposed on white light images of the mice Fig. (**9**). Fluorescence intensity over the heart was significantly greater in the infarcted mice compared to the sham-operated ones.

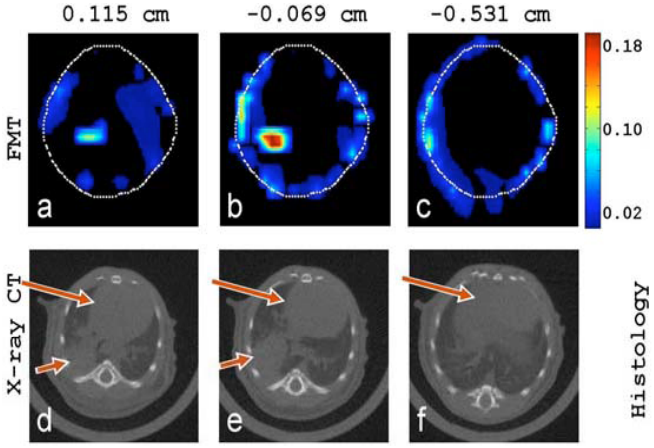

Fig. (8). Tomographic reconstructions of lung and brain tumor in mice (as viewed towards the anterior direction). **a-c**): FMT axial slices of the Angioscence 750 concentration (arb. units) at three different y positions. The white dotted line is the mouse boundary. **d-f**): the corresponding X-ray CT axial slices, small arrows – tumor, big arrows – liver and heart. Reprinted with permission from Ref [54]. ©2009 Society of Photo-Optical Instrumentation Engineers.

Time domain techniques in FMT can further improve the imaging performance by utilizing only the earliest arriving photons arriving to the detector. The "early" photons are those that have had undergone less scattering and therefore followed almost straight line trajectories from the source to the detector. Consequently, Early Photon Tomography (EPT) is less dependent on the ill-posedness of the diffuse inversion scheme and therefore can achieve higher resolution. Niedre *et al.* [56] have demonstrated the performance of this method by *in-vivo* visualization of lung biomarkers at the cellular and molecular level in the same cancer model as above, using both a fluorescent probe sensitive to cathepsin B protease activity (Prosense, Visen Medical), as well as angiogenesis-sensitive fluorescent probe Fig. (**10**). The signals resolved by non-invasive imaging showcased excellent congruence with the corresponding Xray-CT scans. Importantly, FMT images found areas of elevated protease activity associated not only with the primary tumor but also overall with lung tissue which was in clear contradistinction to measurements from control animals. The findings, confirmed by *ex-vivo* imaging and histology and immune-histochemistry studies, indicate that the new method has the potential to non-invasively visualize cellular and molecular signatures through the entire lung *in-vivo*, that could only so far be resolved by destructive histology.

3.4. Bioluminescence Tomography

Both from hardware and image reconstruction perspective, bioluminescence tomography can be considered as a reduced version of FMT because it is not necessary to have an external illumination source to excite the emission. This unavailability of external sources decreases the number of the source-detectors pairs, that reduces the information content of the experimental data set, and makes the tomographic problem more ill-posed. BLT image quality is significantly improved by increasing the diversity of the data set by acquiring images from multiple projections and at multiple wavelengths, together with appropriate reconstruction schemes that incorporate spectral and a-priori known tissue optical properties [57-60].

3.5. Multi-modality Approaches

Optical tomographic systems have been also combined with other imaging modalities such as X-Ray CT or MRI, giving the ability to acquire both an optical reconstruction and a hi-fidelity anatomical image that can be co-registered. Additionally, optical reconstructions can be improved by the incorporation of structural information into the FMT inversion problem [6,9-18]. The anatomical information can be used in making assumptions on the relationship between tissue structures and optical properties and also on the spatial distribution of fluorescent probes. The performance of incorporating a-priori information in the reconstruction has been demonstrated in an *in vivo* imaging study of amyloid-β plaques in transgenic APP23 modeling Alzheimer's disease [61]. The FMT reconstruction of the fluorescent probe signal in the mouse brain, the X-Ray CT, and the corresponding histological slices are presented in Fig. (**11**), demonstrating that multi-modal approaches provide a high degree of both structural and quantitative correlation with ex vivo imaging studies, and are essential for the accurate visualization of neurodegenerative biomarkers *in vivo*.

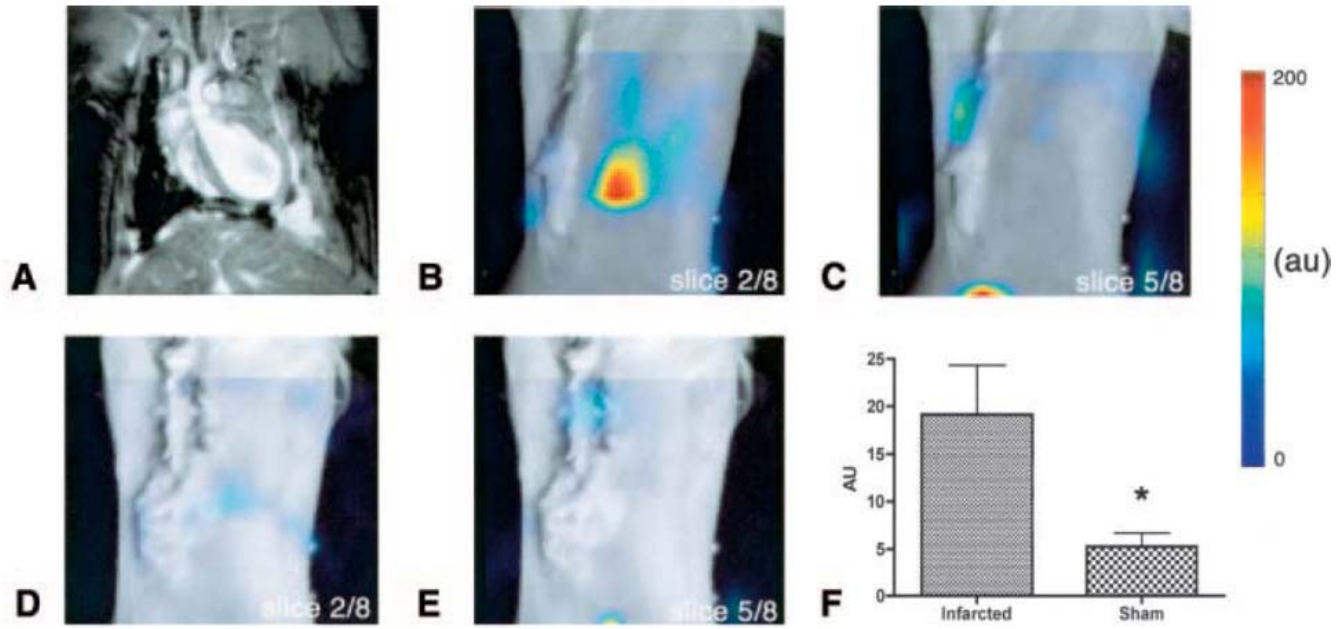

Fig. (9). FMT of myocardial macrophage infiltration *in vivo*. Reconstructed coronal slices from the 3-dimensional FMT data set have been superimposed onto white light images of the mice. Slices 2 to 4 in the FMT data set intersected the heart, slice 1 passed anterior to it, and slices 5 to 8 passed posterior to it. **A**, Long-axis MRI slice in an infarcted mouse corresponding to slice 2 from the fluorescence data set of that mouse (**B**). **C**, Slice 5 from the fluorescence data set of the infarcted mouse. The corresponding slices (**D** - slice 2, **E** - slice 5) of a sham-operated mouse are also shown. Fluorescence intensity over the heart was significantly greater (**P0.05) in the* infarcted mice than the sham-operated mice (**F**). Reprinted with permission from Ref [55]. ©2007

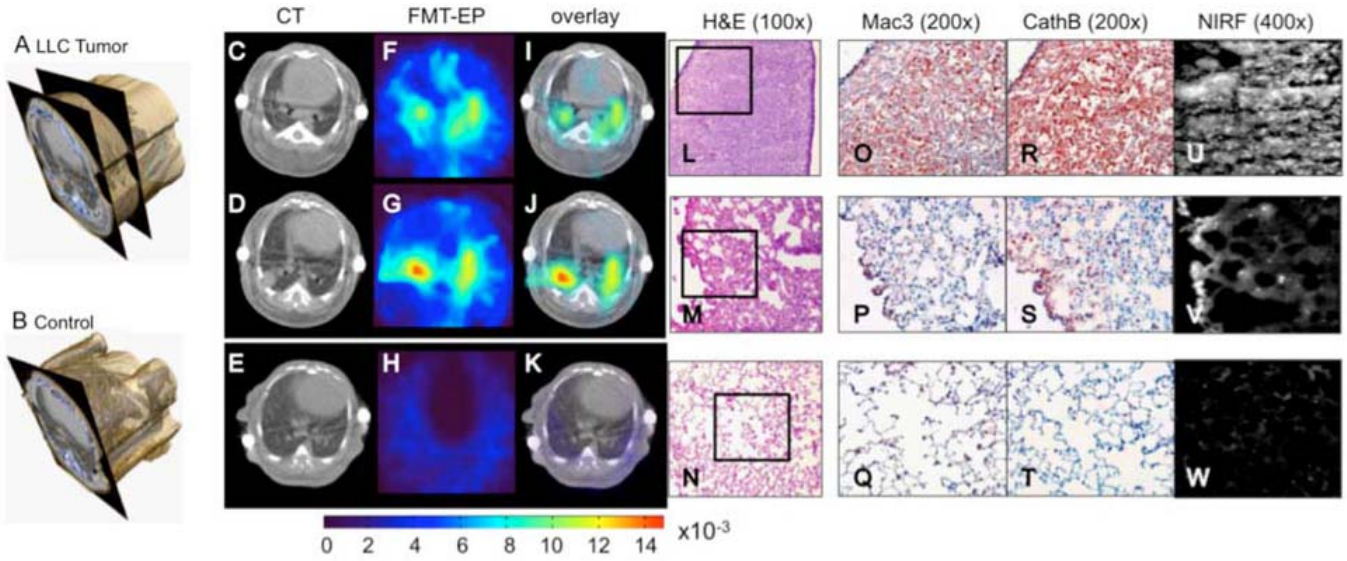

Fig. (10). EPT imaging of a Lewis Lung Carcinoma tumor model in mice. (**A** and **B**) Three-dimensional rendering of a mouse with an LLC tumor 8 days after inoculation and a wild-type control. Mice were injected with a cathepsin-activatable probe (Prosense-750) 24 h before scanning with the EPT system. (**C**–**E**) Selected axial CT slices from the 2 mice. The 2 white circles on either side of the mouse are from the carbon-fiber holder. (**F**–**H**) Axial EPT reconstructions corresponding to the CT slices (arbitrary units). (**I**–**K**) Overlay of the EPT reconstruction on the CT slice. Histology was performed on excised lung samples. (**L**–**N**) H&E stain of tumor, lung tissue that was contralateral to the tumor tissue, and normal lung tissue, respectively. (**O**–**Q**) Macrophage-3 stain and (**R**–**T**) cathepsin B stain of the same tissue. Near-infrared fluorescence (NIRF) microscopy was also performed on adjacent tissue sections (**U**–**W**). The increased macrophage, cathepsin B, and NIRF levels in the primary tumor and the contralateral side corroborates the increased fluorescence signal from the protease-activatable probe measured with the EPT system. As discussed in the text, the increased fluorescence in the contralateral side was primarily due to the host inflammatory response of the lung in response to tumoral challenge as well as microscopic growth of LLC cancer cells into normal tissue. The fluorescent streaks emanating from the side of the animal are reconstruction artifacts. Reprinted with permission from Ref [56]. ©2008.

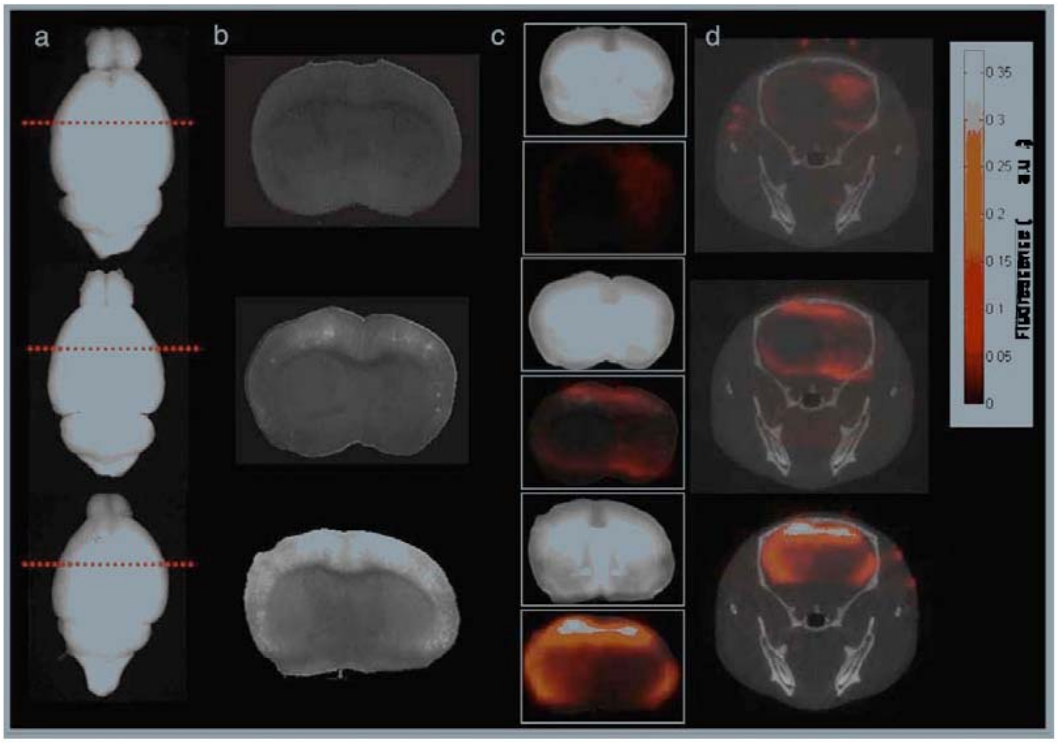

Fig. (11). *Ex vivo* versus *in vivo* FMT imaging comparison for 13 month old C57B/6 control mouse (first row) a 17 month old APP23 tg mouse (Second row) and a 26 month old APP23 tg mouse (third row). (**a**) The first column shows full brain images in the excitation channel using a planar reflectance imaging system. The red dotted line denotes the approximate location corresponding to the slice shown in subsequent columns. (**b**) Planar reflectance images of normalized fluorescence from a single slice are then presented in the second column. (**c**) The third column presents planar images at the excitation wavelength (top) and FMT reconstructions overlaid on normalized planar fluorescence images (bottom). (**d**) *In vivo* multi-modal FMT reconstructions are shown in the final column for a slice corresponding to the same location as the ex vivo images, overlaid on a representative CT slice. All FMT reconstructions are scaled to the same colorbar. Reprinted with permission from Ref [61]. ©2009.

4. OPTOACOUSTIC IMAGING

4.1. Theoretical Background

The optoacoustic effect refers to the induction of acoustic radiation following temperature elevation caused by absorption of light radiation in matter. Usually, the term optoacoustic (or, alternatively, photoacoustic) is related to light-induced phenomena while, in a more general way, creation of sound by either light or microwave (radio frequency) radiation is called thermoacoustics. Here, we solely focus on the imaging of optical contrast therefore the term optoacoustics will be used. Nowadays, vast majority of biomedical optoacoustic imaging applications employ intense pulsed laser sources, leading to the creation of an acoustic wave by an instantaneous light absorption. The magnitude of optoacoustic response is proportional to the local light intensity, optical absorption coefficient, and thermoelastic properties of the imaged tissue while the frequency spectrum of the induced waves is mainly dependent upon the spatial frequency of optical absorption variations and duration of the light pulse. For laser pulse durations in the nanosecond range, a biologically relevant spectrum of optoacoustically-induced signals lies in the ultrasonic spectrum between a few hundreds of kHz and a few tens of MHz [62].

For imaging or sensing purposes, ultrasonic detectors are placed in the vicinity of the imaged object. Similarly to ultrasonic imaging, optoacoustics is a time-resolved method, i.e. time of arrival of the pressure wave directly indicates the distance to the optoacoustic source in the imaged object. If the detector is placed in position $\vec{r}'$, it will sense an integrated pressure wave [63] Fig. (**12**)

$$p(\vec{r}',t)=\frac{\Gamma}{4\pi}\int_V \frac{\partial \psi(\vec{r},t')}{\partial t'}\frac{d^3\vec{r}}{|\vec{r}-\vec{r}'|}\Bigg|_{t'=t-|\vec{r}-\vec{r}'|/v_s} \quad (3)$$

where ψ, Γ, and v_s are power density of the absorbed light, Grüneisen parameter, and acoustic velocity in the medium. Eq. (3) can be interpreted such that, for each time point, the detected pressure variation has been created by integration over all the optoacoustic sources located on a spherical shell of radius $|\vec{r}-\vec{r}'|$ surrounding the detector point $\vec{r}'$ Fig. (**12**).

To further relate the detected optoacoustic pressure variations to the actual optical parameters of tissue, it is convenient to express the absorbed power density ψ in a form of a product between the local absorption coefficient μ_a and light intensity U, i.e. $\psi = \mu_a U$. Since biologically relevant information on tissue as well as bio-marker concentration are

directly linked to the optical absorption, the initial goal of tomographic optoacoustic imaging is reconstruction of optical absorption distribution $\mu_a(\vec{r})$ from a set of measured ultrasonic pressures $p(\vec{r}',t)$. Back-projection algorithms have been so far widely used for volumetric image reconstruction. These algorithms are based on closed-form inversion formulas expressed in two or three dimensions and are analogues to the Radon transform. Back-projection formulas exist for several detection geometries and are implemented either in the spatio-temporal domain [64] or in the Fourier domain [65].

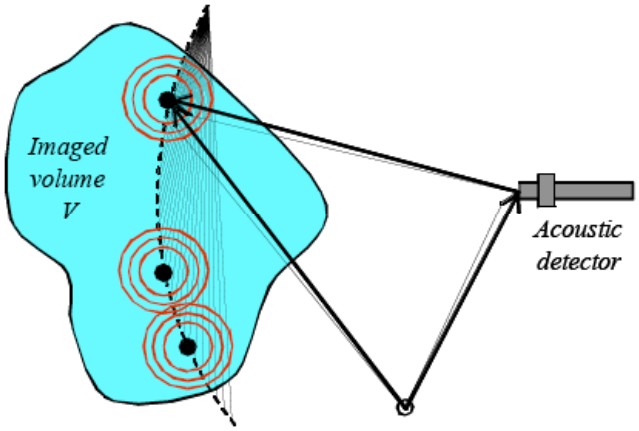

Fig. (12). Schematic representation of optoacoustic signal detection.

Although explicit back-projection algorithms are generally convenient and fast, they are not exact and may lead to the appearance of substantial artifacts in the reconstructed images. A common problem is suppression of slowly varying image components and accentuation of fast changes in the image (small details), which is usually also accompanied by negative optical-absorption values that otherwise have no physical interpretation. In addition, back-projection algorithms are based on an ideal description of the acoustic wave propagation and detection as well as on specific detection geometries, therefore they cannot be easily generalized into a more realistic optoacoustic illumination-detection models that incorporate configuration and instrumentation-dependent factors. Recently, a novel semi-analytical model-based inversion scheme for quantitative optoacoustic image reconstruction was suggested [63], which significantly improves the accuracy and eliminates image artifacts associated with the approximated formulations so that the reconstructed image corresponds to the true energy deposition within the object.

Another reconstruction complication arises from the fact that optoacoustic signals do not directly convey information on the underlying optical absorption coefficient (μ_a) but rather on the local energy absorption in tissue. The latter is proportional to both μ_a and the local light fluence U. In cases of uniform sample illumination, e.g. in cases of superficial imaging where the light sources are uniformly distributed over the object's surface [66], the optoacoustic image approximately reflects the actual map of optical absorption coefficient in tissue. In practice, sample illumination is rarely uniform. For instance, when absorbing targets deeper in tissue are to be imaged, as in whole-body animal or organ imaging, the photon fluence is significantly attenuated as a function of depth and is also significantly affected by tissue optical heterogeneity. Optoacoustic images that are obtained using the assumption of uniform illumination will therefore be biased in favor of targets closer to the surface. Several attempts have been made to overcome this quantification issue. Jetzfellner et al analyzed light attenuation correction schemes based on iterative finite volume modeling approach [67]. A more advanced scheme was recently suggested that relies on the general properties of optical fluence, rather than poorly defined light-propagation model [68]. The method sparsely decomposes the optoacoustic image into two components: a slowly varying global component attributed to the diffusive photon fluence in the medium and a localized high spatial frequency component representing variations of the absorption coefficient. In this way, the method yields quantitative images of both the absorption coefficient and the light fluence.

4.2. Anatomical and Functional Imaging

Due to its hybrid nature, i.e. optical excitation and acoustic detection, the optoacoustic imaging technology benefits both from the rich and versatile optical contrast and high (diffraction-limited) spatial resolution associated with low-scattering nature of ultrasonic wave propagation as compared to photon propagation. To this end, various approaches have attained high fidelity 3D images of *in vivo* vascular anatomy, dynamic microcirculation, and tumor neovascularization with spatial resolutions in the range 20-100 μm and penetration depths of 5 mm and beyond into highly diffuse tissues without introduction of contrast agents [66,69,70]. Optical resolution photoacoustic microscopy (OR-PAM) demonstrated microvasculature images with even better (single capillary) resolution of 5 μm albeit at limited penetration depths (up to 0.7 mm), revealing vasomotion and vasodilation effects non-invasively due to switching between systemic hyperoxia to hypoxia [71]. Besides blood-related contrast, optoacoustics is sensitive to some other intrinsic tissue contrast. For instance, three-dimensional morphology of amyloid plaques and the surrounding microvasculature can be imaged simultaneously through a cranial window without angiographic contrast agents [72] Fig. (**13**). Much like the ultrasound, optoacoustics can form images in real time, currently in 2D [21] but potentially also in 3D [73], therefore it can track fast hemodynamic changes [70]. The two modalities can also be seamlessly integrated into a hybrid imaging device [73].

4.3. Multispectral Optoacoustic Tomography

Indeed, due to the strong hemoglobin absorption, blood vessels naturally have an excellent contrast on optoacoustic images. However, volumetric imaging of photo-absorbing agents would typically require differentiation of these agents on top of spectrally varying background absorption, due to intrinsic tissue photo-absorbers such as hemoglobin and melanin, other chromophores, lipids and water. In response,

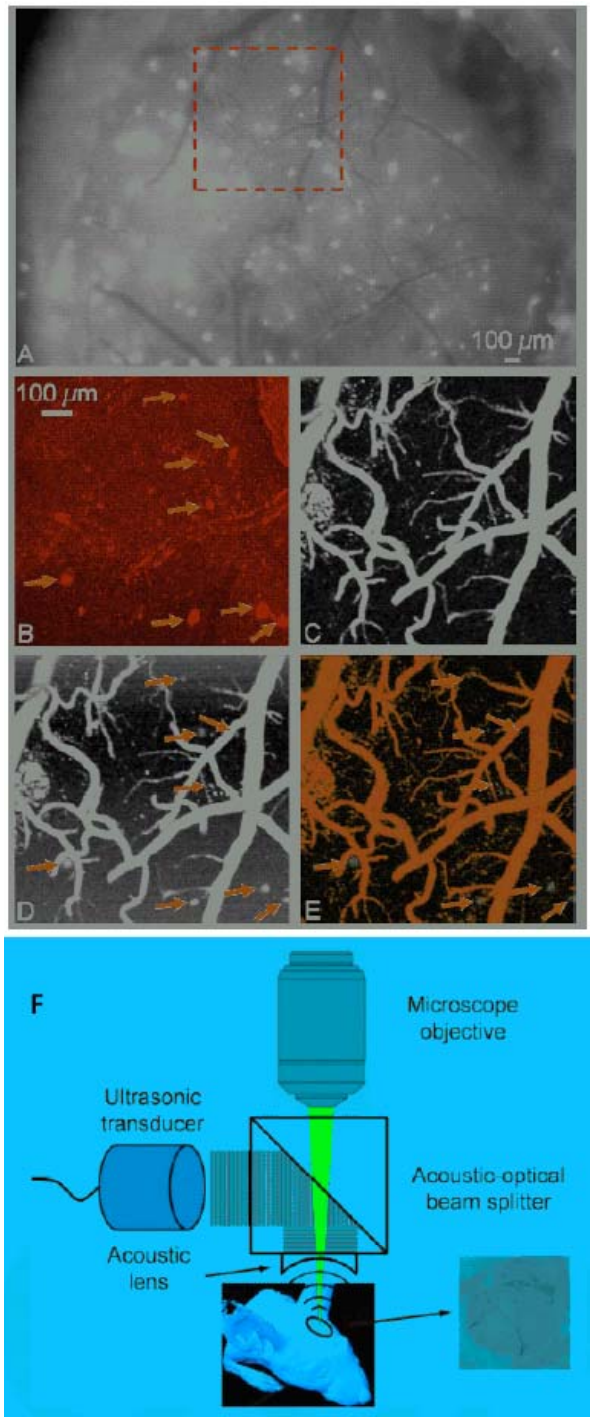

Fig. (13). *In vivo* brain imaging of a Congo-red-injected 10-month-old APP/PS1 mouse through a cranial window. (**A**) Exposed cortical brain region imaged using conventional fluorescence microscopy through the cranial window. The region of interest marked by a red dashed box was imaged by multiphoton microscopy in (**B**), and OR-PAM at 570 nm in (**C**) and 523 nm in (**D**). (**E**) The processed dual-contrast OR-PAM image, where amyloid plaques are colored green (online) and blood vessels are colored red (online). Arrows, plaques. Scale bar in (**B**) applies to parts (**B**)–(**E**). (**F**) Schematic of the optical-resolution photoacoustic microscope for amyloid plaque imaging. ORPAM imaging and multiphoton imaging were performed through a cranial window preparation (inset).

the so-called multi-spectral optoacoustic tomography (MSOT) technique relies on the spectral identification of chromophoric molecules and particles distributed in tissue over background tissue absorption [74,75]. Pulses of different wavelengths are used, in a time-shared fashion, whereas the wavelengths are selected to sample a spectral characteristic in the absorption spectrum of the reporter agent of interest. Agents with absorption spectra that have characteristic differences from the absorption of background tissue are best suited for MSOT imaging. In particular, molecules or nanoparticles with steep absorption changes are optimal, since they can then be resolved by scanning narrow spectral bands. The simplest form of spectral processing is the subtraction between images obtained at two adjacent wavelengths under the assumption that tissue will have a similar absorption at these wavelengths and its effects will cancel out the background absorption and bring out the distribution of the reporter agent and the corresponding tissue biomarker. However, its *in-vivo* use may be problematic since tissues are generally heterogeneous and the tissue absorption has also generally a distinct spectral profile. In this case, the use of more sophisticated spectral processing methods that can separate the spectral signature of reporter agents from that of background absorption may be necessary, especially when baseline measurements are not possible [74]. The spectral decomposition can for instance be done by a simple linear regression method,[20, 21, 76]. Additionally, by employing scanning at different spectral bands, multiple chormophoric molecules or nanoparticles can be resolved in this way during the same imaging session.

The MSOT ability to detect reporter molecules in tissues has been so far showcased by visualizing fluorescent molecular probes, fluorescent proteins and spectrally distinct nanoparticles in mice, fish and other biologically relevant organisms. First animal experiments with MSOT demonstrated the ability to visualize a common fluorescent molecular agent (AlexaFluor 750^{TM}) injected into a mouse [74]. Cross-sectional optoacoustic tomographic reconstructions were acquired at single wavelengths of 750, 770 and 790 nm, revealing an excellent morphological contrast while the MSOT image, generated by spectral processing, simultaneously attained the map of molecular agent distribution in an intact tissue. Later, the method was used to visualize glioblastoma tumor cells stereotactically implanted into mouse brain with the help of IRDye800-c(KRGDf) agent [77], *in vivo* kidney perfusion assisted with the injection of Indocyanine Green [21], and cardiac imaging with gold nanorod contrast [76] Fig. (**14**). Wang *et al*. demonstrated that intravascular MSOT can assess the macrophage-mediated aggregation of nanoparticles and, therefore, identify the presence and the location of nanoparticles associated with macrophage-rich atherosclerotic plaques [78] Fig. (**14**).

High resolution deep tissue imaging of fluorescent proteins (FP) by MSOT was also recently demonstrated [20], which may enable powerful applications in deep-tissue imaging of gene expression. Fig. (**16**) shows results from whole-body visualization of deep-seated fluorescent proteins expressed in diffuse organisms (fly pupae and fishes) with high (mesoscopic) resolution (in this study 38 μm), while simultaneously providing the necessary reference anatomical images. In particular, the images in Fig. (**16(k)-(p)**) were

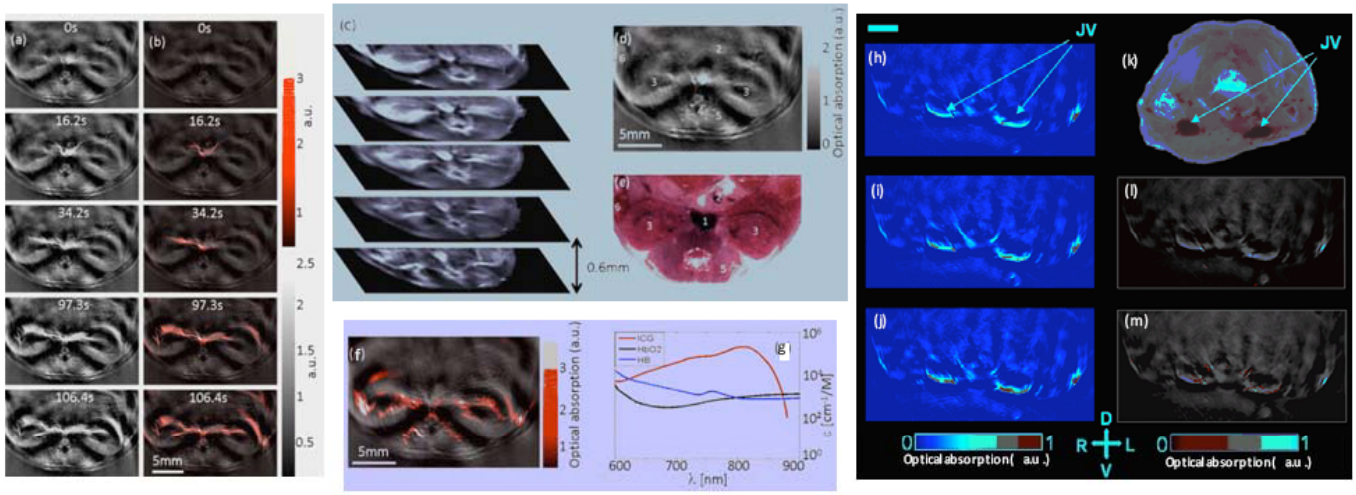

Fig. (14). Real-time volumetric MSOT imaging of contrast agent distribution in living mice. Panels (**a**)-(**g**) show volumetric mouse kidney perfusion MSOT imaging *in vivo*, assisted with an optical contrast agent. (**a**) Crossectional optoacoustic images at different time points of the kidneys of a female CD1 mouse illuminated at 800 nm after having injected 0.33µmoles of ICG. (**b**) Superposition of the difference image and single wavelength image before injection. (**c**) A stack of representative slices of a 3D dataset of the pelvis and kidney region of a female 8 weeks old CD1 mouse. (**d**) Cross-sectional opto-acoustic image before injection of the slice in which the kinetics of ICG was monitored. (**e**) Photograph of a cross-sectional cryoslice at a height corresponding to that shown in (**d**): 1. vena cava, 2. portal vein, 3. kidneys, 4. spinal cord, 5. backbone muscles and 6. spleen. (**f**) Superposition of a single wavelength image (890nm) and the unmixed component corresponding to the ICG signal. (**g**) Molecular extinction coefficient of ICG along with the spectra of oxygenized and deoxygenized hemoglobin. *In vivo* cardiac imaging of a mouse using gold nanorod (AuNR) contrast in jugular veins (JV) is shown in panels (**h**)-(**m**). (**h**) Single-pulse transverse slice through the mouse neck prior to AuNR injection; (**i**) The same slice during injection of AuNR and (**j**) 10 s after finishing the injection of AuNR; (**k**) Photograph of cryosection showing anatomical correspondences; (l) MSOT image before injection; (**m**) MSOT image post injection showing multispectrally resolved distribution of AuNR overlaid on a single wavelength image. Scale bar - 3 mm. Reprinted with permission from Refs [93,94]. ©2010 Optical Society of America.

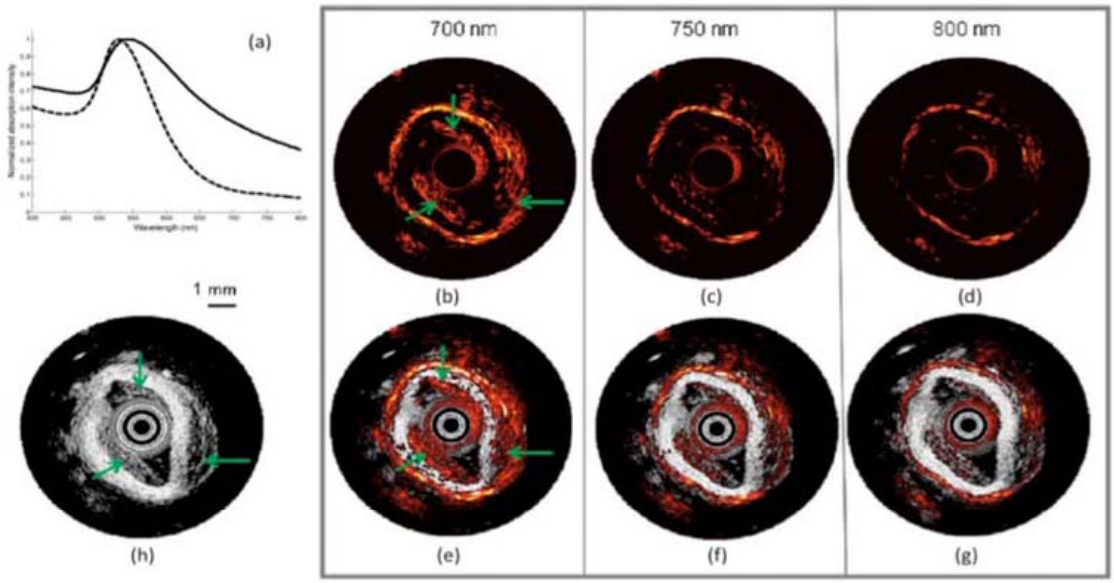

Fig. (15). Multispectral optoacoustic detection of macrophages in atherosclerotic plaques using an absorption spectrum shift of plasmonic gold (Au) nanoparticles (NP). (**a**) Normalized extinction spectra of macrophages loaded with Au NPs (solid line), and Au NPs only (dashed line). Both absorption spectra were normalized with their corresponding maxima. Panels b-h show intravascular ultrasound (IVUS), intravascular photoacoustic (IVPA), and combined IVUS/IVPA images of a diseased rabbit aorta injected with macrophages loaded with Au NPs. The IVUS image is displayed in part b using a 50 dB dynamic range. The injected macrophages in the outer and inner regions of the aorta are denoted in parts b, c, and f with green arrows. The normalized IVPA images (**c-e**) and combined IVUS/IVPA images (**f-h**) obtained using 700, 750, and 800 nm wavelengths are displayed using a 20 dB display dynamic range. The IVPA and combined IVUS/IVPA images taken at 700 nm wavelength (**c-f**) showed a high photoacoustic signal at the injected regions denoted by arrows. Reprinted with permission from ref [78]. ©2009 American Chemical Society.

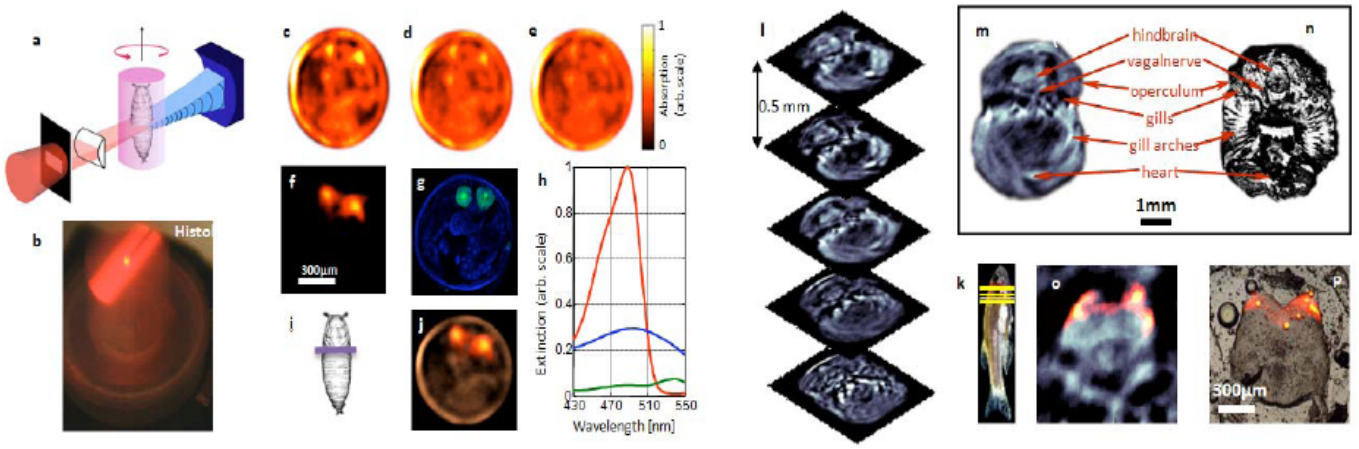

Fig. (16). Multi-spectral optoacoustic tomography of fluorescent proteins *in vivo*. (**a**) Schematic of the experimental setup using selective-plane illumination and confocal detection scheme [96] (red, illuminating light beam; blue, generated ultrasonic waves). (**b**) Top-view photograph of the cylindrically focused beam passing through agar phantom with embedded Drosophila pupae. Panels (**c**)-(**j**) show imaging of eGFP fluorescent protein distribution in Drosophila melanogaster pupa. (**c**)-(**e**) Single-wavelength optoacoustic images acquired at 488 nm, 498 nm and 508 nm; (**f**) Spectrally resolved (MSOT) image of eGFP distribution in an intact pupa; (**g**) Corresponding histology of DAPI-stained pupa at approximately the same imaging plane (green colour corresponds to GFP-expressing salivary glands); (**h**) Extinction spectra of eGFP (red) along with measured absorption of pupa case (blue) and fat areas (green); (**i**) Imaging plane; (**j**) Overlay between the image at 508 nm (**e**) and the spectrally resolved image. Panels (**k**)-(**p**) show three-dimensional *in vivo* imaging through the brain of an adult (6 months old) mCherry-expressing transgenic zebrafish; (**l**) Five cross-sectional optoacoustic imaging slices through the hindbrain area (**k**) of living zebrafish taken at 585 nm. Example of imaged slice and its corresponding histological section are shown in panels (**m**) and (**n**), respectively. (**o**) MSOT image of the brain (zoom-in) with mCherry expression shown in color. (**p**) Corresponding epifluorescence histology made through an excised brain. Reprinted with permission from Ref [20]. ©2009 Macmillan Publishers Ltd.

three-dimensionally (3D) acquired *in-vivo* through the brain of an adult (6 months old) mCherry-expressing transgenic Zebrafish with a cross-section diameter of around 6 mm. The results demonstrate ability to reveal high-resolution molecular activity and superimpose it onto morphological features of identical resolution in the brain of an intact living animal.

Reporter agents with molecular specificity but without large spectral variations can be also opto-acoustically detected using single wavelength measurements; for example agents with slow varying, broad absorption spectra. Examples include peptide or antibody-conjugated gold nanoparticles targeted to EGFR [79] or RGD-conjugated single wall carbon nanotubes with high affinity to $\alpha_v\beta_3$ integrins overexpressed in tumor neovasculature [80] Fig. (**17**). An enzyme-activated chromogenic assay was used in optoacoustic tomography by Li *et al.* with LacZ gene encoding for the X-gal chromogenic substrate [81]. Such detection approaches however would rather rely on the availability of baseline measurements, i.e. images obtained before the appearance of the agent, and are typically appropriate for strongly absorbing agents with fast distribution or expression dynamics.

5. CONTRAST ENHANCEMENT APPROACHES

When reviewing possible approaches for enhancement of contrast for molecular imaging, one has to consider two main enabling components. One is related to the molecular reporter or the label, specific to the biomarker of interest visualized by a certain imaging method. The other part is the actual targeted carrier or contrast agent that produces the necessary signal for this imaging method. Since the main aim here is to review the technological aspects of the various optical and optoacoustic techniques, we will focus on the second component, i.e. the contrast agent. The use of imaging biomarkers has been extensively reviewed elsewhere [1].

Currently, optical molecular imaging is mainly based on fluorescent probes, such as fluorescent dyes and genetic fluorescent reporters (fluorescent proteins). The primary enablers of deep tissue imaging have been indeed the near-infrared fluorochromes, which allow for deeper penetration. More recently, with the introduction of near-infrared fluorescence proteins (IFP) [82], genetic labeling approaches have taken an important step toward their applicability for whole-body *in vivo* imaging in small animals. Yet, a common drawback affecting all fluorescence imaging techniques, and in particular the ones dealing with biological *in vivo* imaging is the presence of a strong autofluorescence background that limits the sensitivity and contrast in the acquired images. Using dyes that are excited in the near infrared part of the spectrum contributes to reduction of this detrimental effect while not completely eliminating it. For further reduction of the auto-fluorescence effects, different subtractions schemes using multispectral approaches have also been developed. One possibility of auto-fluorescence-free imaging is the use of bioluminescence markers, such as the luciferase, however, as discussed, BLT has generally lower performance compared to fluorescence techniques.

An alternative promising approach consists in using instead an upconversion fluorescence principle which is based on the conversion of two or more low energy photons into one photon at higher energy. Due to the lack of tissue autofluorescence in the anti-Stokes part of the spectrum (spectrum below the excitation wavelength), the upconversion principle is very well suited for background-free signal

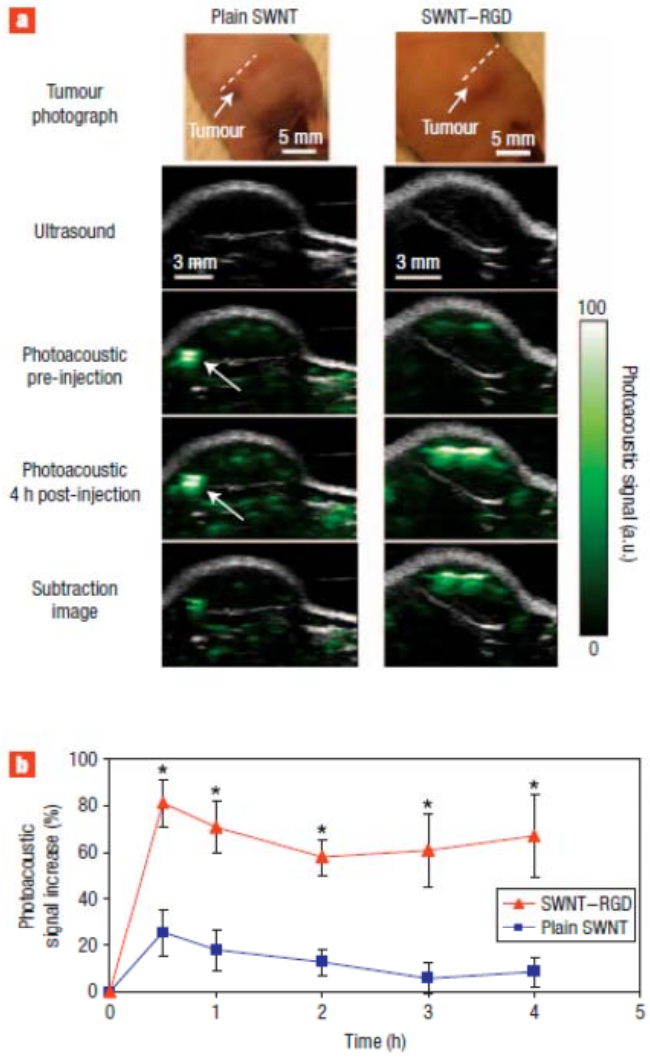

Fig. (17). Single-walled carbon nanotube targets tumour in living mice. (**a**) Ultrasound (grey) and optoacoustic (green) images of one vertical slice (white dotted line) through the tumour. The ultrasound images show the skin and tumour boundaries. Subtraction images were calculated as the 4 h post injection image minus the pre-injection image. The high optoacoustic signal in the mouse injected with plain single-walled carbon nanotubes (indicated with a white arrow) is not seen in the subtraction image, suggesting that it is due to a large blood vessel and not single-walled carbon nanotubes. (**b**) Mice injected with SWNT–RGD showed a significantly higher optoacoustic signal than mice injected with plain single-walled carbon nanotubes. The error bars represent standard error (n=4). Reprinted with permission from Ref [80]. ©2009 Macmillan Publishers Ltd.

imaging allowing potentially to image deeper into tissue with better resolution. Common upconverting materials that have been used nowadays [83- 86] are based on $NaYF_4$ or Y_2O_3 ceramics doped with ytterbium and either erbium or thulium. While usually for two photon fluorescence the absorption cross section is extremely low, for this ceramic materials the absorption of the low energy photons does not involve the presence of any virtual level. This implies an absorption cross section orders of magnitude higher and makes them suitable for planar and fluorescence tomography imaging using standard conventional CW lasers. In order to use the upconverting nanoparticles (UNP) for biological applications, certain criteria need to be satisfied such as low toxicity and water solubility. These conditions have been recently achieved by different groups and in particular by using PEG-coated Y_2O_3 UNPs containing erbium and ytterbium. Both *in vivo* and ex vivo applications have been demonstrated for both microscopy [83-86] and whole animal transillumination planar imaging [84] Fig. (**18**) making them highly promising for future pharmacokinetics studies.

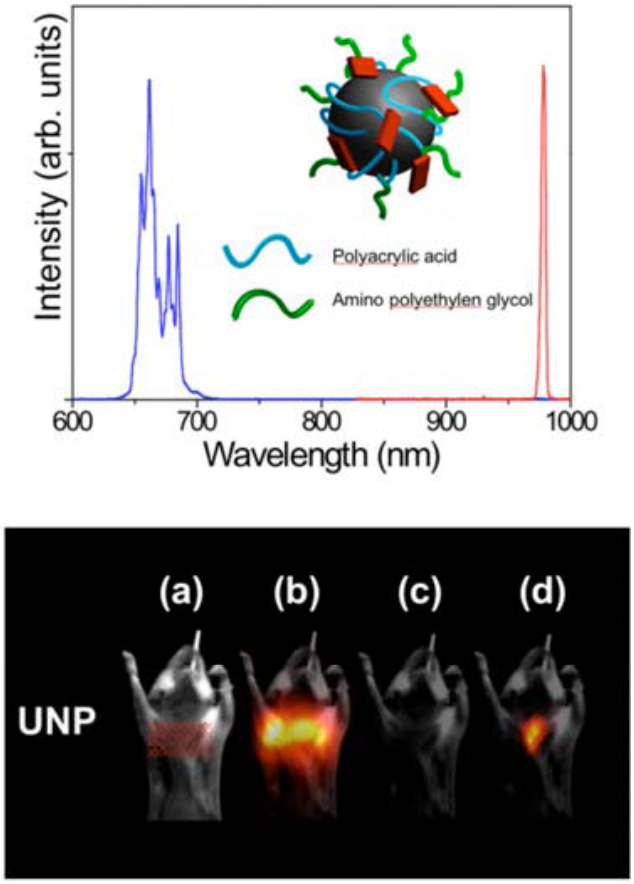

Fig. (18). Top Panel: Emission spectrum of PEG coated Y2O3 upconverting nanoparticles (red line) and excitation wavelength (blue line). Lower Panel: (**a**) White light image of a mouse with a glass capillary tube inserted into the esophagus. The transillumination images averaged over all illumination sources and are presented for the intrinsic excitation wavelength (**b**), the autofluorescence signal (**c**) and the upconversion fluorescence signal (**d**). The lack of autofluorescence signal is evident in (**c**). Reprinted with permission from Ref [84]. ©2009 Optical Society of America.

In optoacoustic imaging, the selection of proper contrast agents seems to be much broader. This is due to the simple fact that, to a certain extent, all materials in nature absorb light therefore can become potential candidates for providing contrast in optoacoustic imaging. For high contrast imaging, of special interest are compounds having high molar extinction coefficient. Several dedicated agents were so far exploited for enhancing contrast in optoacoustics. Due to their large absorption cross-section, carbon and gold-based compounds, such as carbon nanotubes [80], gold nanoparticles

[87], nanoshells [88], nanocages [89] and nanorods [90], have been shown to increase optoacoustic signals *in-vivo* and were further conjugated to provide selective targeting or cancer and inflammation-related events. Optoacoustic imaging of an enzyme-activated chromogenic assay was shown by Li *et al.* with LacZ gene encoding for the X-gal chromogenic substrate [81] have already provided good contrast as well. Some agents used in other non-optical imaging modalities, such as MRI, can potentially be used for creating contrast in optoacoustics and as multimodal agents [91]. Even though many other dedicated contrast agents could potentially be developed for optoacoustic imaging applications, long-term studies may be necessary for examining a variety of efficiency, dosing, safety, and toxicity aspects associated with biological discovery applications or the clinical translation of new contrast agents. The promising recent optoacoustic imaging studies involving quantum dots [92], fluorescent dyes [74,93-95] and fluorescent proteins [20] clearly indicate that these readily commercially available optical agents are in fact a very viable choice for optoacoustics as well. When using fluorescent dyes for optoacoustic imaging, emphasis is given to low quantum-yield fluorochromes with high absorption cross sections, which are particularly useful for optoacoustic signal excitation. Conveniently for optoacoustics, many NIR fluorochromes possess relatively high molar extinction coefficients in excess of 10^5 M^{-1} cm^{-1}, in conjunction with low quantum yield (reduced fluorescence efficiency), acting in favor of optoacoustic signal generation. Many organic fluorochromes exhibit sharp resonances in the vicinity of their peak excitation, making them also spectrally attractive for MSOT applications.

6. CONCLUSIONS

From the various microscopy technologies to endoscopic, intravascular and ocular diagnostic devices, optical imaging unequivocally remains the most versatile and widely used visualization modality in clinical practice and research. In recent years, advances in photonic technologies and image formation methods have received particular attention in biological research and the drug discovery process for non-invasively revealing information on the molecular basis of disease and treatment. An increasing availability of endogenous reporters with physiological and molecular specificity, such as conjugated nanoparticles, genetic reporters, and fluorescent probes, enable insights to cellular and sub-cellular processes through entire small animals, embryos, fish and insects and have revolutionized the role of imaging on the laboratory bench. One of the fundamental reasons to use optical imaging in biomedical research is the wealth of contrast mechanisms that can be offered when exploiting the physical properties of light and the ability to capitalize on a wide range of light-tissue interactions and corresponding photophysical and photochemical mechanisms and processes at the molecular level, i.e. fluorescence, multiphoton absorption, second-harmonic generation, Förster resonance energy transfer, optoacoustics etc. In addition, optical technologies offer a convenient technology for experimentation: Most of the components required can be assembled on the laboratory bench, are modular in design, and can be made portable or compact. High quality of optical components and high detection sensitivity can be nowadays achieved at moderate cost. The utilization of such technologies offers a highly versatile platform for biomedical interrogations that can be used to probe at scales spanning from the molecular to the system level and yield important insights into biology and research.

In this review, we focused on the current progress with instruments and methods for *in-vivo* photonic tomography of whole intact animals and model biological organisms at the molecular level. Indeed, a wealth of new advanced tomographic imaging technologies, suitable for obtaining volumetric visualization of bio-marker distributions in small animals at a whole-body or whole-organ scale, became recently available, an imaging frontier that is not accessible by the conventional tissue-sectioning microscopic techniques due to intensive light scattering beyond the depth of a few hundred microns.

At the level of semi-transparent or *ex vivo* cleared organisms and tissues, techniques like optical projection tomography, selective-plane illumination microscopy and mesoscopic fluorescence tomography offer the capability to obtain molecularly sensitive imaging contrast at high resolution by means of targeted and activatable imaging reporter agents, thus provide a great tool for e.g. investigating the molecular signatures of pathophysiological processes and to study different inflammatory responses as a function of drug dosage. Macroscopic fluorescence imaging is gaining momentum as a molecular imaging method for small-animal whole-body tissue interrogations *in vivo*. It has been long known that light can propagate through several centimeters of tissue in the far-red and near-infrared (NIR). However, light becomes diffuse within a few millimeters of propagation in tissues owing to elastic scattering experienced by photons when they interact with various cellular components, such as the membranes and different organelles. Diffusion results in the loss of imaging resolution. Therefore, macroscopic fluorescence imaging techniques like fluorescence molecular tomography largely depend on spatially resolving and quantifying bulk signals from specific fluorescent entities reporting on cellular and molecular activity. Yet, the combination of advanced macroscopic visualization methods with the ability to impart molecular contrast *in vivo* in whole tissues offers an exciting new tool with large potential in basic research, drug discovery, and clinical application. Currently, these technologies allow for three-dimensional imaging of fluorescence biodistribution in whole animals and are also able to account for tissue optical heterogeneity and the nonlinear dependence of fluorescence intensity on depth and optical properties. A proper combination of optical techniques with conventional techniques like CT and MRI can enhance the ways one can simultaneously and quantitatively monitor structure, function and molecular pathways. Several applications of *in vivo* detection of cellular function and biochemical changes through intact tissues at high sensitivity and molecular specificity were provided in this review, including imaging enzyme up-regulation, carcinogenesis and gene-expression.

Finally, recent advances in optoacoustic technologies hold a great promise of overcoming scattering-related limitations of optical imaging, eventually shifting the paradigm of whole-body molecular imaging towards high resolution real-time performance. Here we described how the novel tomo-

graphic concepts using multispectral optoacoustic tomography (MSOT) are necessary for accurate and high-resolution quantitative molecular investigations in tissues and why it could be potentially a valuable tool for accelerated investigations of therapeutic efficacy and outcome. With the compelling advantages of optical imaging, such as highly diverse contrast mechanisms and easy and safe usability and with imaging performance characteristics that rivals ultrasound in imaging speed, MRI in resolution and nuclear imaging in specificity, MSOT is therefore expected to play a major role in biomedical research and drug discovery applications in the years to come. This is because it brings a new standard of performance in small animal imaging and it can lead to significant niche clinical applications as well, especially in regimes that optical imaging is already an accepted modality, such as endoscopic applications, but possibly also in applications where deeper detection is required. As such, it can play a vital role, from monitoring dynamic phenomena non-invasively to accelerating the decision on potential drug candidates during *in-vivo* screening applications and toxicology animal studies.

REFERENCES

[1] Willmann, J. K.; van Bruggen, N.; Dinkelborg, L. M.; Gambhir, S. S. Molecular imaging in drug development. *Nat. Rev. Drug Discov.*, **2008**, *7* (7), 591-607.

[2] Ntziachristos, V.; Leroy-Willig, A.; Tavitian, B. *Textbook of in vivo Imaging in Vertebrates*. Wiley: New York, **2007**.

[3] Helmchen, F.; Denk, W. Deep tissue two-photon microscopy. *Nat. Methods*, **2005**, *2* (12), 932-940.

[4] Huisken, J.; Swoger, J.; Del Bene, F.; Wittbrodt, J.; Stelzer, E. H. K. Optical sectioning deep inside live embryos by selective plane illumination microscopy. *Science*, **2004**, *305* (5686), 1007-1009.

[5] Sharpe, J.; Ahlgren, U.; Perry, P.; Hill, B.; Ross, A.; Hecksher-Sorensen, J.; Baldock, R.; Davidson, D. Optical projection tomography as a tool for 3D microscopy and gene expression studies. *Science*, **2002**, *296* (5567), 541-545.

[6] Ntziachristos, V.; Tung, C.; Bremer, C.; Weissleder, R. Fluorescence molecular tomography resolves protease activity *in vivo*. *Nat. Med.*, **2002**, *8* (7), 757-760.

[7] Vinegoni, C.; Pitsouli, C.; Razansky, D.; Perrimon, N.; Ntziachristos, V. *In vivo* imaging of Drosophila melanogaster pupae with mesoscopic fluorescence tomography. *Nat. Methods*, **2008**, *5* (1), 45-47.

[8] Ntziachristos, V.; Ripoll, J.; Wang, L. V.; Weissleder, R. Looking and listening to light: the evolution of whole-body photonic imaging. *Nat. Biotechnol.*, **2005**, *23* (3), 313-320.

[9] Brooksby, B.; Jiang, S.; Dehghani, H.; Pogue, B. W.; Paulsen, K. D.; Weaver, J.; Kogel, C.; Poplack, S. P. Combining near-infrared tomography resonance imaging to study *in vivo* and magnetic breast tissue: implementation of a Laplacian-type regularization to incorporate magnetic resonance structure. *J. Biom. Optics.*, **2005**, *10*(5), 051504.

[10] Boas, D. A.; Dale, A. M. Simulation study of magnetic resonance imaging-guided cortically constrained diffuse optical tomography of human brain function. *Appl. Optics*, **2005**, *44* (10), 1957-1968.

[11] Brooksby, B. A.; Dehghani, H.; Pogue, B. W.; Paulsen, K. D. Near-infrared (NIR) tomography breast image reconstruction with a priori structural information from MRI: Algorithm development for reconstructing heterogeneities. *IEEE J. Selected Topics Quantum Electron.*, **2003**, *9* (2), 199-209.

[12] Guven, M.; Yazici, B.; Intes, X.; Chance, B. Diffuse optical tomography with a priori anatomical information. *Phys. Med. Biol.*, **2005**, *50* (12), 2837-2858.

[13] Li, A.; Miller, E. L.; Kilmer, M. E.; Brukilacchio, T. J.; Chaves, T.; Stott, J.; Zhang, Q.; Wu, T.; Chorlton, M.; Moore, R. H.; Kopans, D. B.; Boas, D. A. Tomographic optical breast imaging guided by three-dimensional mammography. *Appl. Optics*, **2003**, *42* (25), 5181-5190.

[14] Schweiger, M.; Arridge, S. R. Optical tomographic reconstruction in a complex head model using a priori region boundary information. *Phys. Med. Biol.*, **1999**, *44* (11), 2703-2721.

[15] Lin, Y.; Gao, H.; Nalcioglu, O.; Gulsen, G. Fluorescence diffuse optical tomography with functional and anatomical a priori information: feasibility study. *Phys. Med. Biol.*, **2007**, *52*, 5569-5585.

[16] Davis, S. C.; Dehghani, H.; Wang, J.; Jiang, S.; Pogue, B. W.; Paulsen, K. D. Image-guided diffuse optical fluorescence tomography implemented with Laplacian-type regularization. *Optics Express*, **2007**, *15* (7), 4066-4082.

[17] Gulsen, G.; Birgul, O.; Unlu, M. B.; Shafiiha, R.; Nalcioglu, O. Combined diffuse optical tomography (DOT) and MRI system for cancer imaging in small animals. *Technol. Cancer Res. Treat.*, **2006**, *5* (4), 351-363.

[18] Intes, X.; Maloux, C.; Guven, M.; Yazici, B.; Chance, B. Diffuse optical tomography with physiological and spatial a priori constraints. *Phys. Med. Biol.*, **2004**, *49* (12), N155-N163.

[19] Razansky, D.; Vinegoni, C.; Ntziachristos, V. Multispectral photoacoustic imaging of fluorochromes in small animals. *Opt. Lett.*, **2007**, *32* (19), 2891-2893.

[20] Razansky, D.; Distel, M.; Vinegoni, C.; Ma, R.; Perrimon, N.; Koster, R.; Ntziachristos, V. Multispectral opto-acoustic tomography of deep-seated fluorescent proteins *in vivo*. *Nat. Photonics*, **2009**, *3* (7), 412-417.

[21] Buehler, A.; Herzog, E.; Razansky, D.; Ntziachristos, V. Video rate optoacoustic tomography of mouse kidney perfusion. *Optics Lett.*, **2010**, *35* (14), 2475-2477.

[22] Deguchi, J.; Aikawa, M.; Tung, C. H.; Aikawa, E.; Kim, D. E.; Ntziachristos, V.; Weissleder, R.; Libby, P. Inflammation in atherosclerosis: visualizing matrix metalloproteinase action in macrophages *in vivo*. *Circulation*, **2006**, *114*, 55-62. Tanaka, E.; Choi, H. S.; Fujii, H.; Bawendi, M. G.; Frangioni, J. V. Image-guided oncologic surgery using invisible light: completed pre-clinical development for sentinel lymph node mapping. *Ann. Surg. Oncol.*, **2006**, *13* (12), 1671-1681.

[23] Ware, R. W.; Lopresti, V. 3-dimensional reconstruction from serial sections. *Intl. Rev. Cytology-a Survey Cell Biol.*, **1975**, *40*, 325-440.

[24] Weninger, W. J.; Mohun, T. Phenotyping transgenic embryos: a rapid 3-D screening method based on episcopic fluorescence image capturing. *Nat. Genet.*, **2002**, *30* (1), 59-65.

[25] Ewald, A. J.; McBride, H.; Reddington, M.; Fraser, S. E.; Kerschmann, R. Surface imaging microscopy, an automated method for visualizing whole embryo samples in three dimensions at high resolution. *Dev. Dynamics*, **2002**, *225* (3), 369-375.

[26] Sarantopoulos, A.; Themelis, G.; Ntziachristos, V. Three dimensional multispectral cryo-slicing. *Mol. Imag. Biol.*, **2010**.

[27] Alanentalo, T.; Asayesh, A.; Morrison, H.; Loren, C. E.; Holmberg, D.; Sharpe, J.; Ahlgren, U. Tomographic molecular imaging and 3D quantification within adult mouse organs. *Nat. Methods*, **2007**, *4* (1), 31-33.

[28] Sharpe, J. Optical projection tomography. *Annu. Rev. Biomed. Engin.*, **2004**, *6*, 209-228.

[29] Vinegoni, C.; Razansky, D.; Figueiredo, J.; Nahrendorf, M.; Ntziachristos, V.; Weissleder, R. Normalized Born ratio for fluorescence optical projection tomography. *Opt. Lett.*, **2009**, *34* (3), 319-21.

[30] Vinegoni, C.; Feruglio, P. F.; Cortez-Retamozo, V.; Razansky, D.; Medoff, B. D.; Ntziachristos, V.; Sbarbati, A.; Pittet, M.; Weissleder, R. Imaging of molecular probe activity with Born-normalized fluorescence optical projection tomography. *Optics Lett.*, **2010**, *35* (7), 1088-1090.

[31] Vinegoni, C.; Fexon, L.; Feruglio, P. F.; Pivovarov, M.; Figueiredo, J. L.; Nahrendorf, M.; Pozzo, A.; Sbarbati, A.; Weissleder, R. High throughput transmission optical projection tomography using low cost graphics processing unit. *Optics Exp.*, **2009**, *17* (25), 22320-22332.

[32] Dodt, H. U.; Leischner, U.; Schierloh, A.; Jahrling, N.; Mauch, C. P.; Deininger, K.; Deussing, J. M.; Eder, M.; Zieglgansberger, W.; Becker, K. Ultramicroscopy: three-dimensional visualization of neuronal networks in the whole mouse brain. *Nat. Methods*, **2007**, *4* (4), 331-336.

[33] Mahmood, U.; Tung, C. H.; Bogdanov, A.; Weissleder, R. Near-infrared optical imaging of protease activity for tumor detection. *Radiology*, **1999**, *213* (3), 866-870.

[34] Bugaj, J. E.; Achilefu, S.; Dorshow, R. B.; Rajagopalan, R. Novel fluorescent contrast agents for optical imaging of *in vivo* tumors

based on a receptor-targeted dye-peptide conjugate platform. *J. Biomed. Optics*, **2001**, *6* (2), 122-133.

[35] Ntziachristos, V.; Turner, G.; Dunham, J.; Windsor, S.; Soubret, A.; Ripoll, J.; Shih, H. A. Planar fluorescence imaging using normalized data. *J. Biomed. Optics*, **2005**, *10* (6). 064007.

[36] Zacharakis, G.; Shih, H.; Ripoll, J.; Weissleder, R.; Ntziachristos, V. Normalized transillumination of fluorescent proteins in small animals. *Mol. Imaging*, **2006**, *5* (3), 153-159.

[37] Kak, A.; Slaney, M. *Principles of computerized tomographic imaging*. IEEE Press: New York, **1999**.

[38] Ishimaru, A. Wave propagation and scattering in random media. IEEE Press: New York, **1997**.

[39] Xu, Y.; Iftimia, N.; Jiang, H. B.; Key, L. L.; Bolster, M. B. Imaging of *in vitro* and *in vivo* bones and joints with continuous-wave diffuse optical tomography. *Optics Express*, **2001**, *8* (7), 447-451.

[40] Ntziachristos, V.; Weissleder, R. Charge-coupled-device based scanner for tomography of fluorescent near-infrared probes in turbid media. *Med. Physics*, **2002**, *29* (5), 803-809.

[41] Brooksby, B.; Jiang, S. D.; Dehghani, H.; Pogue, B. W.; Paulsen, K. D.; Kogel, C.; Doyley, M.; Weaver, J. B.; Poplack, S. P. Magnetic resonance-guided near-infrared tomography of the breast. *Rev. Scientific Instruments*, **2004**, *75* (12), 5262-5270.

[42] Graves, E. E.; Ripoll, J.; Weissleder, R.; Ntziachristos, V. A submillimeter resolution fluorescence molecular imaging system for small animal imaging. *Med. Physics*, **2003**, *30* (5), 901-911.

[43] Schulz, R. B.; Peter, J.; Semmler, W.; D'Andrea, C.; Valentini, G.; Cubeddu, R. Comparison of noncontact and fiber-based fluorescence-mediated tomography. *Optics Lett.*, **2006**, *31* (6), 769-771.

[44] Deliolanis, N.; Lasser, T.; Hyde, D.; Soubret, A.; Ripoll, J.; Ntziachristos, V. Free-space fluorescence molecular tomography utilizing 360 degrees geometry projections. *Optics Lett.*, **2007**, *32* (4), 382-384.

[45] Corlu, A.; Choe, R.; Durduran, T.; Lee, K.; Schweiger, M.; Arridge, S. R.; Hillman, E. M. C.; Yodh, A. G. Diffuse optical tomography with spectral constraints and wavelength optimization. *Appl. Optics*, **2005**, *44* (11), 2082-2093.

[46] Srinivasan, S.; Pogue, B. W.; Dehghani, H.; Leblond, F.; Intes, X. Data subset algorithm for computationally efficient reconstruction of 3-D spectral imaging in diffuse optical tomography. *Optics Exp.*, **2006**, *14* (12), 5394-5410.

[47] Hielscher, A. H.; Bluestone, A. Y.; Abdoulaev, G. S.; Klose, A. D.; Lasker, J.; Stewart, M.; Netz, U.; Beuthan, J. Near-infrared diffuse optical tomography. *Dis. Markers*, **2002**, *18* (5-6), 313-337.

[48] Choe, R.; Corlu, A.; Lee, K.; Durduran, T.; Konecky, S. D.; Grosicka-Koptyra, M.; Arridge, S. R.; Czerniecki, B. J.; Fraker, D. L.; DeMichele, A.; Chance, B.; Rosen, M. A.; Yodh, A. G. Diffuse optical tomography of breast cancer during neoadjuvant chemotherapy: A case study with comparison to MRI. *Med. Phys.*, **2005**, *32* (4), 1128-1139.

[49] Brooksby, B.; Pogue, B. W.; Jiang, S. D.; Dehghani, H.; Srinivasan, S.; Kogel, C.; Tosteson, T. D.; Weaver, J.; Poplack, S. P.; Paulsen, K. D. Imaging breast adipose and fibroglandular tissue molecular signatures by using hybrid MRI-guided near-infrared spectral tomography. *Proc. Natl. Acad. Sci.USA*, **2006**, *103* (23), 8828-8833.

[50] Oleary, M. A.; Boas, D. A.; Li, X. D.; Chance, B.; Yodh, A. G. Fluorescence lifetime imaging in turbid media. *Optics Lett.*, **1996**, *21* (2), 158-160.

[51] Paithankar, D. Y.; Chen, A. U.; Pogue, B. W.; Patterson, M. S.; SevickMuraca, E. M. Imaging of fluorescent yield and lifetime from multiply scattered light reemitted from random media. *Appl. Optics*, **1997**, *36* (10), 2260-2272.

[52] Jiang, H. B. Frequency-domain fluorescent diffusion tomography: a finite-element-based algorithm and simulations. *Appl. Optics*, **1998**, *37* (22), 5337-5343.

[53] Ntziachristos, V.; Weissleder, R. Experimental three-dimensional fluorescence reconstruction of diffuse media by use of a normalized Born approximation. *Optics Lett.*, **2001**, *26* (12), 893-895.

[54] Deliolanis, N. C.; Dunham, J.; Wurdinger, T.; Figueiredo, J. L.; Tannous, B. A.; Ntziachristos, V. *In-vivo* imaging of murine tumors using complete-angle projection fluorescence molecular tomography. *J. Biomed. Optics*, **2009**, *14* (3), 3.

[55] Sosnovik, D. E.; Nahrendorf, M.; Deliolanis, N.; Novikov, M.; Aikawa, E.; Josephson, L.; Rosenzweig, A.; Weissleder, R.; Ntziachristos, V. Fluorescence tomography and magnetic resonance imaging of myocardial macrophage infiltration in infarcted myocardium *in vivo*. *Circulation*, **2007**, *115* (11), 1384-1391.

[56] Niedre, M. J.; de Kleine, R. H.; Aikawa, E.; Kirsch, D. G.; Weissleder, R.; Ntziachristos, V. Early photon tomography allows fluorescence detection of lung carcinomas and disease progression in mice *in vivo*. *Proc. Natl. Acad. Sci. USA*, **2008**, *105* (49), 19126-19131.

[57] Wang, G.; Li, Y.; Jiang, M. Uniqueness theorems in bioluminescence tomography. *Med. Phys.*, **2004**, *31* (8), 2289-2299.

[58] Gu, X. J.; Zhang, Q. H.; Larcom, L.; Jiang, H. B. Three-dimensional bioluminescence tomography with model-based reconstruction. *Optics Exp.*, **2004**, *12* (17), 3996-4000.

[59] Dehghani, H.; Davis, S. C.; Jiang, S. D.; Pogue, B. W.; Paulsen, K. D.; Patterson, M. S. Spectrally resolved bioluminescence optical tomography. *Optics Lett.*, **2006**, *31* (3), 365-367.

[60] Klose, A. D.; Beattie, B. J.; Dehghani, H.; Vider, L.; Le, C.; Ponomarev, V.; Blasberg, R. *In vivo* bioluminescence tomography with a blocking-off finite-difference SP3 method and MRI/CT coregistration. *Med. Phys.*, **2010**, *37* (1), 329-338.

[61] Hyde, D.; de Kleine, R.; MacLaurin, S. A.; Miller, E.; Brooks, D. H.; Krucker, T.; Ntziachristos, V. Hybrid FMT-CT imaging of amyloid-beta plaques in a murine Alzheimer's disease model. *Neuroimage*, **2009**, *44* (4), 1304-1311.

[62] V. W. L. *Photoacoustic Imaging and Spectroscopy*. CRC Press: Boca Raton, Florida, **2009**.

[63] Rosenthal, A.; Razansky, D.; Ntziachristos, V. Fast semi-analytical model-based acoustic inversion for quantitative optoacoustic tomography. *IEEE Trans Med. Imaging*, **2010**, *29* (6), 1275 - 1285.

[64] Kruger, R. A.; Liu, P. Y.; Fang, Y. R.; Appledorn, C. R. Photoacoustic Ultrasound (PAUS) - Reconstruction Tomography. *Med. Phys*, **1995**, *22* (10), 1605-1609.

[65] Köstli, K.; Frenz, M.; Bebie, H.; Weber, H. Temporal backward projection of optoacoustic pressure transients using fourier transform methods. *Phys. Med. Biol.*, **2001**, *46* (7), 1863-72.

[66] Zhang, E.; Laufer, J.; Pedley, R.; Beard, P. *In vivo* high-resolution 3D photoacoustic imaging of superficial vascular anatomy. *Phys. Med. Biol.*, **2009**, *54* (4), 1035-1046.

[67] Jetzfellner, T.; Razansky, D.; Rosenthal, A.; Schulz, R.; Englmeier, K.; Ntziachristos, V. Performance of iterative optoacoustic tomography with experimental data. *Appl. Phys. Lett.*, **2009**, *95* (1), 013703.

[68] Rosenthal, A.; Razansky, D.; Ntziachristos, V. Quantitative optoacoustic signal extraction using sparse signal representation. *IEEE Trans Med. Imaging*, **2009**, *28* (12), 1997-2006.

[69] Wang, X.; Pang, Y.; Ku, G.; Xie, X.; Stoica, G.; Wang, L. Noninvasive laser-induced photoacoustic tomography for structural and functional *in vivo* imaging of the brain. *Nat. Biotechnol.*, **2003**, *21* (7), 803-806.

[70] Song, L.; Maslov, K.; Wang, L. V. Section-illumination photoacoustic microscopy for dynamic 3D imaging of microcirculation *in vivo*. *Optics Lett.*, **2010**, *35* (9), 1482-1484.

[71] Hu, S.; Maslov, K.; Wang, L. V. Noninvasive label-free imaging of microhemodynamics by optical-resolution photoacoustic microscopy. *Opt. Exp.*, **2009**, *17* (9), 7688-7693.

[72] Hu, S.; Yan, P.; Maslov, K.; Lee, J.; Wang, L. Intravital imaging of amyloid plaques in a transgenic mouse model using optical-resolution photoacoustic microscopy. *Opt. Lett.*, **2009**, *34* (24), 3899-3901.

[73] Niederhauser, J.; Jaeger, M.; Lemor, R.; Weber, P.; Frenz, M. Combined ultrasound and optoacoustic system for real-time high-contrast vascular imaging *in vivo*. *IEEE Trans Med. Imaging*, **2005**, *24* (4), 436-40.

[74] Razansky, D.; Vinegoni, C.; Ntziachristos, V. Multispectral photoacoustic imaging of fluorochromes in small animals. *Opt. Lett.*, **2007**, *32* (19), 2891-2893.

[75] Ntziachristos, V.; Razansky, D. Molecular Imaging by Means of Multispectral Optoacoustic Tomography (MSOT). *Chem. Rev.*, **2010**, *110* (5), 2783-2794.

[76] Taruttis, A.; Herzog, E.; Razansky, D.; Ntziachristos, V. Real-time imaging of cardiovascular dynamics and circulating gold nanorods with multispectral optoacoustic tomography. *Optics Exp.*, **2010**, *17* (24), 21414-21426.

[77] Li, M.-L.; Oh, J.-T.; Xie, X.; Ku, G.; Wang, W.; Li, C.; Lungu, G.; Stoica, G.; Wang, L. V. Simultaneous molecular and hypoxia imaging of brain tumors *in vivo* using spectroscopic photoacoustic tomography. *Proc. IEEE* **2008**, *96* (3), 481-489; Li, M.-L.; Oh, J.-T.;

X. X.; G, K.; Wang, W.; Li, C.; Lungu, G.; Stoica, G.; Wang, L. V. Simultaneous molecular and hypoxia imaging of brain tumors *in vivo* using spectroscopic photoacoustic tomography. *Proc. IEEE,* **2008**, *96* (3), 481-489.

[78] Wang, B.; Yantsen, E.; Larson, T.; Karpiouk, A.; Sethuraman, S.; Su, J.; Sokolov, K.; Emelianov, S. Plasmonic intravascular photoacoustic imaging for detection of macrophages in atherosclerotic plaques. *Nano. Lett.,* **2009**, *9* (6), 2212-2217.

[79] Mallidi, S.; Larson, T.; Aaron, J.; Sokolov, K.; Emelianov, S. Molecular specific optoacoustic imaging with plasmonic nanoparticles. *Opt. Exp.,* **2007**, *15* (11), 6583-6588.

[80] De la Zerda, A.; Zavaleta, C.; Keren, S.; Vaithilingam, S.; Bodapati, S.; Liu, Z.; Levi, J.; Smith, B.; Ma, T.; Oralkan, O.; Cheng, Z.; Chen, X.; Dai, H.; Khuri-Yakub, B.; Gambhir, S. Carbon nanotubes as photoacoustic molecular imaging agents in living mice. *Nat. Nanotechnol.,* **2008**, *3* (9), 557-562.

[81] Li, L.; Zemp, R.; Lungu, G.; Stoica, G.; Wang, L. Photoacoustic imaging of lacZ gene expression *in vivo*. *J. Biomed. Opt.,* **2007**, *12* (2), 020504.

[82] Shu, X.; Royant, A.; Lin, M.; Aguilera, T.; Lev-Ram, V.; Steinbach, P.; Tsien, R. Mammalian expression of infrared fluorescent proteins engineered from a bacterial phytochrome. *Science,* **2009**, *324* (5928), 804-807.

[83] Hilderbrand, S. A.; Shao, F. W.; Salthouse, C.; Mahmood, U.; Weissleder, R. Upconverting luminescent nanomaterials: application to *in vivo* bioimaging. *Chem. Commun.,* **2009**, (28), 4188-4190.

[84] Vinegoni, C.; Razansky, D.; Hilderbrand, S.; Shao, F.; Ntziachristos, V.; Weissleder, R. Transillumination fluorescence imaging in mice using biocompatible upconverting nanoparticles. *Opt. Lett.,* **2009**, *34* (17), 2566-2568.

[85] Nyk, M.; Kumar, R.; Ohulchanskyy, T. Y.; Bergey, E. J.; Prasad, P. N. High contrast *in vitro* and *in vivo* photoluminescence bioimaging using near infrared to near infrared up-conversion in TM3+ and Yb3+ doped fluoride nanophosphors. *Nano. Lett.,* **2008**, *8* (11), 3834-3838.

[86] Wu, S. W.; Han, G.; Milliron, D. J.; Aloni, S.; Altoe, V.; Talapin, D. V.; Cohen, B. E.; Schuck, P. J. Non-blinking and photostable upconverted luminescence from single lanthanide-doped nanocrystals. *Proc. Natl. Acad. Sci. USA,* **2009**, *106* (27), 10917-10921.

[87] Rayavarapu, R.; Petersen, W.; Ungureanu, C.; Post, J.; van Leeuwen, T.; Manohar, S. Synthesis and bioconjugation of gold nanoparticles as potential molecular probes for light-based imaging techniques. *Int. J. Biomed. Imaging*, **2007**, *2007*, 29817.

[88] Wang, Y. W.; Xie, X. Y.; Wang, X. D.; Ku, G.; Gill, K. L.; O'Neal, D. P.; Stoica, G.; Wang, L. V. Photoacoustic tomography of a nanoshell contrast agent in the *in vivo* rat brain. *Nano. Lett.,* **2004**, *4* (9), 1689-1692.

[89] Song, K.; Kim, C.; Cobley, C.; Xia, Y.; Wang, L. Near-infrared gold nanocages as a new class of tracers for photoacoustic sentinel lymph node mapping on a rat model. *Nano. Lett.,* **2009**, *9* (1), 183-188.

[90] Eghtedari, M.; Oraevsky, A.; Copland, J.; Kotov, N.; Conjusteau, A.; Motamedi, M. High sensitivity of *in vivo* detection of gold nanorods using a laser optoacoustic imaging system. *Nano. Lett.,* **2007**, *7* (7), 1914-1918.

[91] Bouchard, L.; Anwar, M.; Liu, G.; Hann, B.; Xie, Z.; Gray, J.; Wang, X.; Pines, A.; Chen, F. Picomolar sensitivity MRI and photoacoustic imaging of cobalt nanoparticles. *Proc. Natl. Acad. Sci. USA,* **2009**, *106* (11), 4085-4089.

[92] Shashkov, E. V.; Everts, M.; Galanzha, E. I.; Zharov, V. P. Quantum dots as multimodal photoacoustic and photothermal contrast agents. *Nano. Lett.,* **2008**, *8* (11), 3953-3958.

[93] A. B.; E. H.; D. R.; V. N. Video rate optoacoustic tomography of mouse kidney perfusion. *Optics Lett.,* **2010**, *35*(14),2475-2477

[94] A. T.; E. H.; D. R.; V. N. Real-time Imaging of Cardiovascular Dynamics and Circulating Gold Nanorods with Multispectral Optoacoustic Tomography. *Optics Express,* **2010**, *18*(19),19592-19602

[95] Ma, R.; Taruttis, A.; Ntziachristos, V.; Razansky, D. Multispectral optoacoustic tomography (MSOT) scanner for whole-body small animal imaging. *Optics Exp.,* **2009**, *17* (24), 21414-21426.

[96] Razansky, D.; Vinegoni, C.; Ntziachristos, V. Imaging of mesoscopic-scale organisms using selective-plane optoacoustic tomography. *Phys. Med. Biol.,* **2009**, *54* (9), 2769-2777.

Received: June 28, 2010 **Accepted: November 07, 2010**